Temporal changes of organic carbon accumulation and anthropogenic influences in the outer Oslofjord, Loperen

A micropaleontological and geochemical study of the benthic environment

Jimmy K. Papadopoulos

Master Thesis
Environmental Geosciences - Environmental Stratigraphy
60 credits

Institute of Geosciences
The Faculty of Mathematical and Natural Sciences

UNIVERSITY OF OSLO

09/15/2020

Temporal changes of organic carbon accumulation and anthropogenic influences in the outer Oslofjord, Loperen

A micropaleontological and geochemical study of the benthic environment

Jimmy K. Papadopoulos

Master Thesis
Environmental Geosciences - Environmental Stratigraphy
60 credits

Institute of Geosciences
The Faculty of Mathematical and Natural Sciences

UNIVERSITY OF OSLO

09/15/2020

Abstract

Stratigraphic profiles of two sediment cores stationed at Loperen are analyzed to distinguish temporal changes of accumulation rates of total organic carbon (TOC) in at least the last four centuries. The aim is to investigate potential anthropogenic influences that have impacted the water quality in the area by monitoring these trends, including carbon-nitrogen ratios (C/N), heavy metals analysis, and micropaleontological assessment of benthic faunal taxa. The trends of metal concentration peaks and radiometric dating to approximate the absolute and relative age of the cores. TOC content is residue of past biota that can have an affect on marine primary production, eutrophication, oxygen conditions and finally benthic fauna. TOC in recent years has increased at Loperen, in the Hvaler area. Reaching a "moderate status" in table 4-1, with accumulation of > 2.7 % TOC in 2018 and 2019. Micropaleontological assessment of species of benthic foraminifera are indicators for ecological quality status (EcoQS) that aid as a proxy for relative changes in the quality of the bottom water of the channel. These methods are useful to correlate reference conditions to present-day of Loperen and the surrounding areas.

Acknowledgements

I would like to thank Elisabeth Alve for giving me the opportunity to join this project and be an inspiration for enthusiasm through this endeavor. I would also like to give an equal thanks to Silvia Hess for putting in the extra time to guide me through the program. They both have given me excellent insight over the years, helped me to grow, as well as allowed me to have a taste of the forefront of innovative strategies for environmental sciences. I cannot even begin to express my gratitude of your help even after the Covid-19 pandemic in March. Silvia took the risk of entering the lab to save some samples and Elisabeth pushed administration to give me more time for thesis in order to proof. If that is not a sight for inspiration and leadership, I do not know what is.

I also will not forget to thank, PhD student Anouk Tosca Klootwijk, who was an extremely valuable source of insight, eager to help and a strong motivational speaker in a great time of need. Many thanks to Mufak Naoroz for the providing extensive information on lab procedures and all the extra time he took helping in the lab as well. I would also like to thank Magnus Kristoffersen for help in lab work and information.

A special thanks to Aud Helland, for co-supervising and providing wonderful insights on the Trygve Braarud. Another special thanks Skipper Sindre Holm, and the Trygve Braarud crew members Yan Sundoe, Leif-Arild Huseby for all their help and hospitality. I really had an unforgettable time. I would also want to mention much appreciation for Karl Johan Ullavik Bakken in administration, for pushing out of his comfort zone to allow me the extra time needed to stay on my feet during the crisis.

I could not have done this without everyone mentioned, nor could I have done this without my best friend and flat mate in SiO housing, Erdem Lamazhapov, for motivating me and helping me proof-read my thesis on very short notice. Also, the two people who supported me from the beginning, my Mom and Dad. Thank you for being my beacon of light from 6500 km away.

Table of Contents

List of figures and tables:

depth and C: represents the C/N ratio vs. depth.

Figure 4.6 Heavy metal concentrations relative to depth. Dashed lines represent recent dates around peaks and the 17th to 19th centuries. Arrows represent changes in EcoQS for Cd, Ni, Cr, Cu, Pb, and Zn (Table 4-1) with depth. The colored arrows pointing at the trend line indicate the initial EcoQS from the surface depth, and the next arrow downcore indicates the point of change in EcoQS. Hg is analyzed semi-quantitatively because the values are below the detectable limit of the ICP-MS and do not accurately represent EcoQS. The ratio between mercury concentrations (mg/kg) still provide an accurate trend in relation to depth.

Figure 4.7.1 Two graphs are shown. Faunal density per gram sediments vs. depth – time and relative abundance (%) vs. depth-time. Ecological group classifications: EG I (very sensitive) C to EG V (very resilient).

Figure 4.7.2 Biotic indices for foraminifera present for NQI, H'log, ES100 and AMBI. EcoQS colors are represented on the graphs are rake from Table 4-1 above.**Figure 4.7.3** The Dendrogram is based on Bray Curtis similarity cluster diagram. It represents similarities between foraminifera assemblages relative to depth. The dates are assigned to each depth based on radioisotopes from Appleby, 2019 and interpolated and extrapolated dates.

Figure 4.7.4 Multi-dimensional similarity (MDS) plot of benthic foraminifera assemblages from each sample (depth) based on relative abundance data. Assemblages are: C. laevegata (EG I), B. marginata (EG III), S. fusiformis and N. stella (EG V).

Figure 5.1 Sand sediment accumulation rates (g m^{-2} y^{-1}) relative to depth.

Figure 5.3 Temporal changes of TOC accumulation rates vs depth in relation to TN

Table 3-1 JP-19 station core and depth to sediment surface (m), equipment used, subsampling and measurements,
sample treatments, and geographical coordinates.

Table 4-1 EcoQS classification of biotic indices (Veileder, 2013) and metal concentrations (Veileder, 2016). Foram AMBI classification (Borja et al 2000) (Alve et al. 2016). TOC % environmental classification (Molvaer et al. 1997). "High" represents reference conditions and shifting toward "Bad" represents very poor Conditions (Bouchette, 2018).

1 Introduction

Most visitors come to Norway to witness the wonderous scenery painted by geomorphological processes. From diversely undulating landmasses between mountains and lowlands surrounded by vast coastlines stretching across the countryside. With fjords designed by countless Millenia of transitioning ice ages, adjusting glacial movement, and continuously plowing new and unique landscapes. Not only is it a sight for visitors, but the coastal areas and fjords are a great and ever-growing attraction to those who live in the country. Coastal waters are great not only to balance out temperatures as opposed to the hinterlands but is also the market supply 90% of global fish catch (Wolanski, 2007). The fjords along the coasts can simply be defined as estuaries with distinct boundaries that were affected by glaciation at one time (Svytski & Shaw, 1995). The fjord thresholds or sills, usually at mouth of fjords, are the strongest indicators that the fjords origin by glacial scouring through threshold relative stability and glacial retreat (Holtedahl, 1967; Shoemaker, 1986). These sills are formed by the glaciers lack of erosion forcing the glacier to spread out across valleys and lowlands with less sediment swept away at its terminus upon retreat (Holtedahl, 1967; Shoemaker, 1986).

Estuaries are generally defined as buffer zones for the inflow of fluvial freshwater are mixed with saltwater oceanic currents that may be affected by tidal oscillations. The mixing of marine and freshwater make estuaries vulnerable to all sorts of changes in the aquatic environment as well as anthropogenic influences (Wolanski, 2007; Svytski & Shaw, 1995). Estuaries and continental shelves encompass over 5% of earth surface and approximately 2% of the oceanic volume (Wolanski, 2007). However, these estuaries and coasts are among the most populated areas, making up 60% of human populations (Lindeboom 2002). As global populations have been estimated to double worldwide every 30-50 years, the rate of population growth at coasts is far greater, estimated to double every 20 years because of human migrations away from hinterlands (Wolanski, 2007). The expansion of aquaculture has also imposed pressure on the ecosystem by restricting waterflow of estuaries, forced physical and chemical changes to sediment, eutrophication leading to oxygen depletion and affecting the benthic ecosystem (Crossland et al. 2006). The North Sea alone, has had fisheries catch 30-40% of its fish biomass anually, with the peak of farm exploitation recorded in 1996 with estimations reaching 3.5×10^6 t (Lindeboom, 2002).

Although fjords are less than 0.1% of the surface of the oceans, they are still considered carbon burial “hotspots,” where carbon accumulation rates are 5 times faster than other marine systems (Keil, 2015). This accounts for 11% of the annual carbon burial for the ocean floor, making it far

more impactful than originally meets the eye (Keil, 2015). Some other examples besides aquaculture that have been affecting carbon accumulation rates, are land clearing by overgrazing, use of fertilizer, poor farming, food processing industries, domestic sewage, deforestation leading to sediment erosion (Wolanski, 2007; Alve, 1996). When the biomass of organic material and sediment loads run off into local river, it can change shorelines from sandy to muddy as well as increase turbidity and nutrient richness in estuaries, leading to eutrophication as a result. (Wolanski, 2007; Alve 1996). This leads to phytoplankton overgrowth as another marker for carbon accumulation, e.g. C. polylepis blooms in Scandinavian waters in the late 80's that outcompeted other algae through toxicity and ultimately reducing oxygen levels in the marine environment. (Helland et al. 2002).

The expansion of aquaculture has also imposed pressure on the ecosystem by restricting waterflow of estuaries, forced physical and chemical changes to sediment, eutrophication leading to oxygen depletion and affecting the benthic ecosystem (Crossland et al. 2006). The North Sea has fisheries catch 30-40% of its annual fish biomass, with the peak of farm exploitation recorded in 1996 with estimations reaching 3.5×10^6 t (Lindeboom, 2002).

Since the last two centuries post-industrial revolution, changes in contamination levels, status of benthic fauna, and physical and chemical characteristics of marine environments have led to significant changes in composition for accumulating sediments (IAEA, 2003). European countries have faced anthropogenic impacts due to this industrial revolution and population increases that was only firstly mitigated through legislation by the European Union (EU) in the 1970's. The EU and member states, The European Commission and Norway had come up with a long-term agreement to protect all water resources with implementing the Water Framework Directive (WFD) in the year 2000 (Directive, 2000/60/EC; WFD, 2014). Crucial analysis of anthropogenically impacted sediment sinks can aid in reconstructing models of historical changes to aid in remediation strategies in restoring the environment to background (reference) conditions (IAEA, 2003; Alve 2009). Reference conditions can be defined as high status biological qualities comparable to pre-impacted or nearly unimpacted times (Alve et al. 2009).

Benthic foraminifera are microorganisms that have previously been used as proxies to understand pollution in marine waters, as they are known to respond quickly to changes in the environment (Alve, 1996). Additionally, benthic foraminifera calcium carbonate tests preserve in the sediment, therefore they can be used to reconstruct changes in environmental conditions through time. The retrospective records of foraminifera, their relative abundance, tolerant or opportunistic species in

combination with diversity indices ($Hlog_2$, ES_{100}) may determine whether pollution is relating to oxygen depletion or ecological quality status (EcoQS) in the environment (Alve, 1996; Bouchet et al. 2012; Dolven et al. 2013).

The aim in this study is to evaluate the EcoQS of Loperen, by analyzing temporal changes in the benthic foraminifera assemblages, as well the total organic carbon (TOC) flux and heavy metal (HM) concentrations in the sediment cores. Loperen is an understudied location that will give us new insights to anthropogenic influences that are characterized by the Glomma river down to the Hvaler area. Analyzing the sediment core samples at station JP-19 will help us to evaluate the history up to present day organic carbon matter circulation and how climate changes may have affected nutrient transport.

2 Study area

2.1 Loperen, Hvaler

The Oslofjord is the 7th longest fjord in Norway which stand at a length of approximately 100 km. (Nesje, 2009) The entire Oslofjord system has an area of approximately 1644 km^2 starting southwest around Larvik, reaching up to Oslo and back southeast to the Swedish border. The Oslofjord system is separated into three parts, the inner and outer Oslofjord, as well as the Drammensfjord. Drammensfjord connects northwest with the inlet being the Drammen river, and has an outlet to the south sill of the fjord. The inner Oslofjord is also a sill fjord consisting of Vestfjord to the west and Bunnefjord to the east. The Vestfjorden is separated by the Drobak sill to the South, where it meets with the outer Oslofjord (Pub. 193, 2007; Staalstrøm & Ghaffari, 2015). The sill at the outer Oslofjord's meets Skagerrak and is a plateau that lies between Larvik and Koster at a depth of 125m.

The outer Oslofjord, which connects to Hvaler has an area of approximately 1405 km^2 and an average depth of 70 m. The Hvaler (Whales) basin runs as deep as 460-465 (Staalstrøm & Ghaffari, 2015; Helland 2002). The mouth of the Glomma river dissipates as it meets Fredrikstad, contributing to the Glomma estuary. The Glomma estuary then contributes to Hvaler in northerneastern Skagerrak (Staalstrøm & Ghaffari, 2015: Pub 193, 2007). Hvaler makes up a collection of islands and islets which follows the inner coastal passage and accesses Loperen (figure 2.1)(Pub. 193, 2007). The name Loperen comes from the word Laupa, "run;" describing how it is "the one that runs across" the passage dividing Hvaler islands Amaloy and Kirkoy and leading south to outer Loperen passed the Hvaler tunnel (Thorsnæs, 2015; Pub. 193, 2007). The length of

the Loperen channel measures at approximately 5 km in length and the water depth maximum measured depth from the records are 71m at the JP-19 station.

Figure 2.1 This map identifies Loperen at the tip of the red mark on the map. Loperen is the channel passing between Hvaler Islands and Singlefjorden. Modified photo of Trygve Braarud radar and Earth Explorer maps and satellite image of Norway and Sweden. Modified map from USGS.gov Earth Explorer website 2019 (earthexplorer.usgs.gov).

2.2 Hydrography and pollution history of Hvaler area

The following water masses described are based on Danish and Norwegian algorithms of mean surface distribution between 1996 and 2000, according to Kristiansen and Aas, 2014. Due to marine circulation, various major water masses mix into the Hvaler area from Kattegat. Mean surface distribution of Atlantic water is estimated at 30-40 % between the border of Sweden and Loperen area. In addition, water masses arriving from Kattegat is 10-15% Baltic sea water for the entire Hvaler area and approximately 0-5% German bight or Norwegian river water (Kristiansen & Aas, 2014).

Mean surface distribution of salinity is estimated at 27-28 PSU for the Hvaler area and

approximately one percent less than the outer Oslofjord likely due to inflow of river freshwater (Kristansen & Aas, 2014). The CTD results for Loperen, Hvaler are in figure 2.2.1 below.

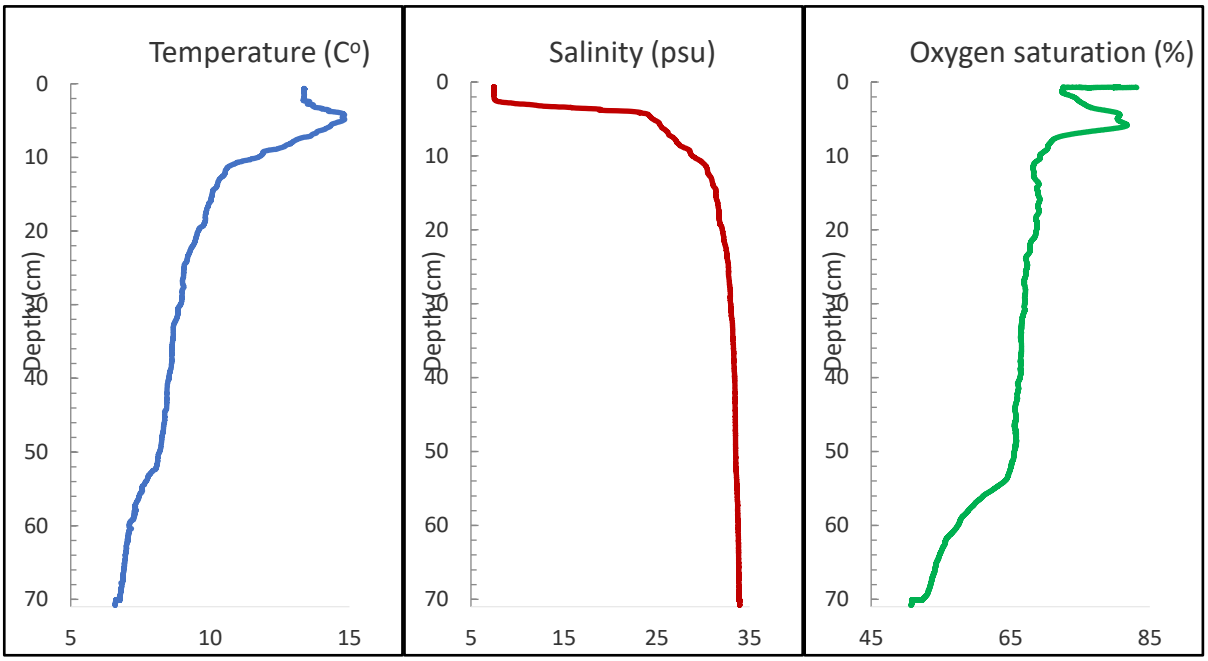

Figure 2.2.1: Temperature (C°), salinity (psu) and oxygen saturation from the CTD measurements at JP-19 station on the research vessel, June 26, 2019.

The Glomma river is one of the longest and widest rivers in Norway. Where frequent flooding occurs due to heavy precipitation, coupled with narrowing sections, increasing velocities and perpetual overflows (Anja Sundal, Per. Comm. June 6, 2019). When comparing neighboring rivers (Drammens river and Alta river) in Southeast Norway, Glomma has greater annual discharge and flux of TOC (Helland et al. 2003).

Although Glomma floods often, events between 1990 to 1994 still showed linear trend of improvement in the general water quality over the last 10 years (Faafeng et al. 1996). A strongly impactful flood period with peaks around mid-June of 1995, brought attention to the risk of registered and unregistered landfills that could transport nutrient rich sediment to the estuary and Hvaler (figure 2.2.2; Faafeng et al. 1996). Past core records have shown a drastic increase in sedimentation rates that year, reaching as high as 3 g cm^{-2} y^{-1} at the north section of outer Loperen due to the flooding (Rygg, 1996). Studies at the end of September that year show that flood period at Saprsfossen (Sarps falls near Sarpsborg) was recorded at a 10 times higher sedimentation accumulation rate than any of the prior flood periods over the last 5 years (Faafeng et al. 1996). Algae growth was slowed due to a lack of significant phosphorus being transported and the flooded areas had low light and low salinity conditions, abnormal blooms were present in areas of the outer

Oslofjord due to increase in nitrate and silicate concentrations that were effectively utilized by the aglae (Faafeng et al. 1996).

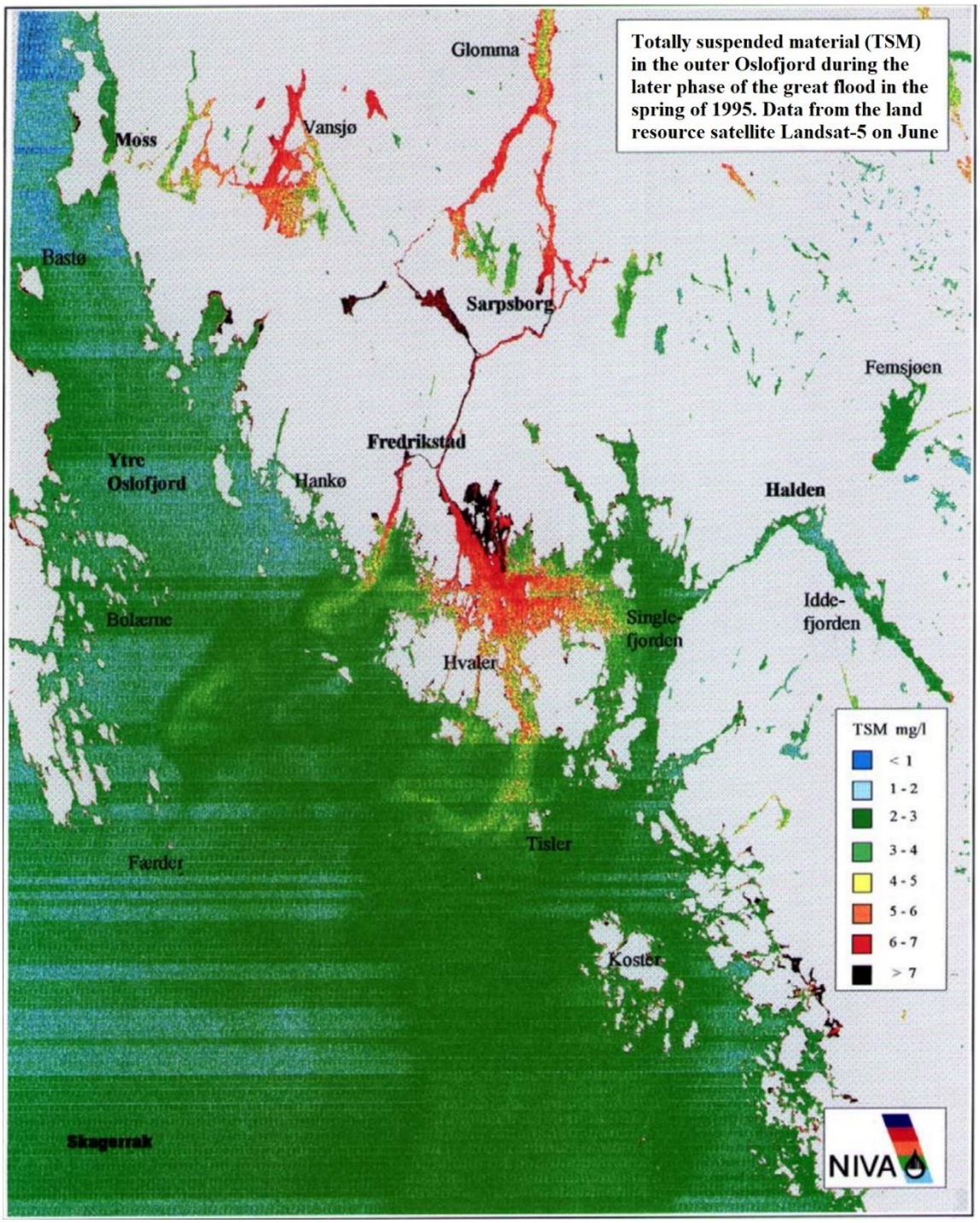

Figure 2.2.2: Satellite image of the distribution of particles and surface temperature. This model displays total suspended material (TSM) from the Glomma, into the Hvaler area. Particles passing through Loperen are ejected toward Outer Loperen as they change direction via current. Modified and translated TSM model created by Faafeng et al. 1996, Niva report.

3 Materials and methods

3.1 Sample collection and preparations

The research vessel used for sample collection (Appendix C) is the Trygve Braarud. The plan was to collect samples in Loperen close to previous stations (3SPI and NIWA) to potentially compare temporal accumulation rates, geochemical and micropaleontological records if applicable. The vessel is equipped with multiple GPS and navigational radar systems, including euronav seapro (figure 2.1), to locate the site of interest. The Multibeam echosounder was used to avoid steeper slopes on the west side of the channel, and to attempt to avoid areas with more physical disturbances that may affect the integrity of the core samples. The station JP-19 was finally chosen inside the lower central portion of the Loperen area, slightly closer to the east side of the channel located beside stations 3SPI and NIWA as shown figure 2.1.

Figure 3.1 Neil Brown Conductivity-Temperature-Depth (CTD) instrument on the Trygve Braarud. Photo taken on the Trygve Braarud courtesy of Silvia Hess (2019-06-26).

The instruments used for sample collections of the stations were the Neil Brown Conductivity-Temperature-Depth (CTD), Gemini gravity corer and Abdullah corer (UiO, 2018). The CTD was used to measure depth from water surface to the marine strata. As it descends 0.5 m/s, it also collects levels of oxygen, temperature, and salinity (Figure 2.Appendix G).

Table 3-1: JP-19 station core and depth to sediment surface (m), equipment used,

subsampling and measurements, sample treatments, and geographical coordinates.

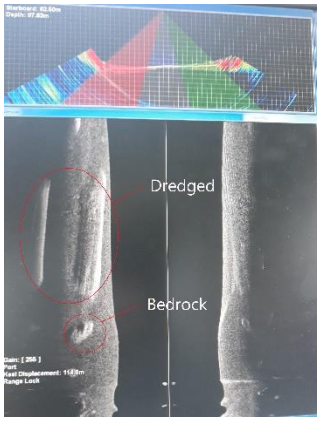

Core *dept	Equipment	Sampling (cm)	Sample Treatment	Coordinates
JP-19P (71 m)	CTD, Gemini corer	0 - 20 cm 1 cm slices 20 - 66 cm 2 cm slices	stored in freezer/ Freeze dry	59°03.300' N 10°58.120' E
JP-19Abd (71 m)	Abdullah corer	50 - 82 cm 2 cm slices 82 - 137 cm 5 cm slices	stored in freezer/ Freeze dry	59°03.300' N 10°58.120' E

Figure 3.2: Radar on the Trygve Braarud detecting past dredging and bedrock.

The Gemini gravity corer is a twin corer with an internal diameter of 8 cm, which allow additional weights to be added based on sediment hardness and penetration difficulties. The Abdullah corer is single cylinder with a core liner of 2 meters length and relatively smaller. It is meant to provide a longer sediment record without additional weights applied, versus the Gemini corer. The narrow diameter and deeper sediment record provided by the Abdullah corer is at greater risk of being less reliable due to potential shortening (Dück et al. 2019). Both a fully weighted Gemini corer and the Abdullah corer were lowered at approximately 1.0 m/s. Lowering the core when exceeding core speeds are discouraged in order to avoid core shortening when penetrating the sediment surface (Morton et al. 1997). Out of 12 Gemini core replicates (Appendix C), the JP-19P replicate was chosen for containing the least visible bioturbation coupled with the greatest relative depth. The first Abdullah core sample was collected and kept for further sampling. All subsamples at the JP-19 station were sectioned with horizontal slices. JP-19P subsamples were taken from surface to bottom core, at either 1 or 2 cm slices. JP-19Abd samples begin from 50 cm to bottom core, at 2 or 5 cm intervals respectively (Table 3-1). Samples of both stations were collected in plastic containers, placed in a freezer on deck and immediately taken for freeze drying at the lab for subsampling and further analysis.

3.2 Water content (WC)

The JP-19P and JP-19Abd station samples were collected and immediately placed in a freezer to maintain water content (WC) and prepare for freeze drying at the lab. The wet weight of each frozen sample was recorded. The sample were transferred to a vacuum chamber to freeze dry samples through sublimation.

Low pressure freeze drying is a rapid and simple method preferred to eliminate moisture and loosen sediment characteristics as opposed to heat drying. Heat drying may likely harden the soil and cause physical damage or destroy crystal lattices of the sediment making it harder to handle in lab (Charm, 1967).

Every batch of samples were dried for approximately three days. Each batch of dry samples were immediately weighed and recorded to avoid significant levels of water molecules returning to the sample and interfering with measurements. The dry weight was subtracted from the wet weight of the soil to retrieve % WC (Flemming et al. 2000). Water content % was measured to delineate between natural occurring compaction of sediments or physical disturbances that may have affected the sample integrity (Dück et al. 2019).

3.3 Grain size analysis

For grain size analysis, subsamples were selected from specific intervals to reduce processing time, with very little reduction on data resolution (Appendix D). The weight of each subsample was approximately one gram and contained in glass vials. The sediment subsamples were passed through a 1000 μm sieve without force, then dry stirred to lightly break down aggregates before further processing. The sediments were prepared for 3 to 5 minutes of sonication. Approximately 0.20 grams of sediments were placed in a beaker and mixed with a solution of 5% Calgon ($NaPO_3$) for deflocculation (Naoroz, M. 2018), which supplies dispersive cations to excess particles surrounding the sediments (Wintermyer et al. 1955). The grain size particulates were measured through a Laser Diffraction Particle Size Analyzer – Single Wave Beckman Coulter LS 13 320 SW model (ISO 13320, 2009). After sonication was complete, the solution was then poured into the LS 13 320 SW analyzer, where the particles in the solution were suspended in deionized water.

The function of the LS 13 320 SW is to quantify approximately 90% of each particulate in the solution. As the laser scatters off the particles, multiple detectors record the angle of diffraction and separates them based on size (PN B05577AB, 2011). The particle range measured by the laser anylzer was between 0.04 μm, and as large as 2000 μm in diamater. Auto-alignment and background auto-recalibrations were run before every sample (ISO 13320, 2009). The procedure was successfully run twice and the average value between the two runs were calculated.

3.4 Radio-Isotopic dating

Approximately 4 grams of sediment was extracted from all 70 subsamples from JP-19P and JP-

19Abd sediment cores. They were sent to the Liverpool University Environmental Radioactivity Laboratory where a select number of subsamples were selected and dated due to financial limitations. The following was based on the literature of Appleby (2019) – Appendix A. Radioactive isotopes ^{210}Pb, ^{226}Ra, and ^{137}Cs were analyzed in the sediment by direct gamma assay using Ortec HPGe GWL series well-typed coaxial low background intrinsic germanium detectors (Appleby et al. 1986). The ^{210}Pb isotope was determined by gamma emissions at 46.5keV energy. The radioactive isotope ^{226}Ra was determined 295 keV gamma emissions followed by 352 keV energy by radioactive equilibration of 3 weeks storage of ^{226}Ra leading to daughter radionuclide ^{214}Pb. ^{137}Cs was measured by the highest energy output of 662keV (Appleby, 2019).

Recent dating chronologies that reliably capture up to 150 years use leads natural radioactive isotope ^{210}Pb with a 22.3 years half-life. Both constant rate of ^{210}Pb supply (CRS) and constant initial concentration (CIC) models were used. CRS model detects the dilution of ^{210}Pb in sediment laminae and the CIC was appropriate for determining based on the degree of variability of the sedimentation rate and discontinuity of the sediment record in the CRS model. ^{137}Cs was used as an independent verification of dates in the sediment record. Self-absorption of gamma emissions effects within the sample, allows for corrections to be made in the sediment record (Appleby, 1992). Interpolated dates were found by median age between direct dating. The extrapolated dates were measured assuming constant sediment accumulation rates between 1904 and 1816 as shown in figure 4.4 B. Raw data for direct, interpolated and extrapolated dates are shown in Appendix F.

3.5 Total organic carbon (TOC) and total nitrogen (TN) content

The TOC and TN analysis is in accordance to the standard of the United States Environmental protection Agency (Schumacher, 2002). The first step was to weigh approximately 3 grams of sediments for TOC and TN subsampling for JP-19P, and JP-19Abd. The samples were pulverized in a mortar until at least 2.5 g of fine powder was produced. After every sample, the mortar was cleaned with ethanol and paper towels. Approximately 1 gram of pulverized sediment was transferred into a labeled centrifuge tube for TOC. Around 15 to 16 ml of 10% hydrochloric acid (HCl) was added to remove the inorganic carbonates. The sample was then placed on a shaker for 2 hours and centrifuged at 3000 rpm for 10 minutes to let the sediment settle at the bottom of the tube. Afterwards, the centrifuged solution was decanted, and the sediment rinsed with distilled water and stirred to complete a single acid wash. The rinsing process followed by centrifuging and decantation was done a total of 3 times to clean the sediment thoroughly of inorganic compounds

and to raise the pH until it was considered close enough to neutral (over pH 5). The sample was then heat dried for two days at 40 °C, removed from the heat and left until room temperature for proper weighing (Schumacher, 2002). The weight was recorded, and the sample was removed from the centrifuge tube and pulverized once again. Approximately 12 to 15 mg of of the newly processed material was transferred into tin crucibles to be wrapped air-tightly, and sent to the organic elemental analyzer (Naoroz, Per. Comm. Feb 2020).

The Thermo scientific Flashsmart CHNS/O analyzer determines the amount of organically bound elements, such as organic carbon and nitrogen, by complete combustion of a sample in a tin crucible at approximately 1800 °C. It can analyze the amount of the elemental gases produced, which then results in retrieving the TOC and TN content (BS EN 13137, 2001). One sample was processed at each interval shown in Appendix D, through the elemental analyzer. Three tests were run between filter changes and different core depths (14.5 cm, 63 cm and 129.5 cm - Appendix D) to provide a record of consistency in the results.

TOC was corrected by taking the total carbon measured multiplied by the correction factor. The correction factor was taken by the equation:

$$(Weight_{TOCtreated} / Weight_{TOCuntreated}) = \text{correction factor}$$

3.6 Heavy metal (HM) concentrations

Using a small container labeled JP-19 with approximately 2.5 grams of pulverized sediments left, 1 gram of the pulverized material was transferred into a 50 ml polypropylene centrifuge tube. Approximately 20 ml of distilled 7M nitric acid (HNO3) was added and mixed thoroughly to dissolve the bioavailable fraction of metals. The tubes were shaken to homogenize the solution with the sediments and heated in a 120°C pressurized autoclave for 30 minutes to fully dissolve the metals. The samples were then centrifuged for 10 minutes at 4000 rpm to separate the dissolved metals solution from the sediment. The metal solution was further diluted by taking out approximately 0.20 ml of metal solution and adding 1% HNO3 until the solution reached a total of 10 ml. The approximate dilution factor of 50 (1:49). Finally, the Inductive Coupled Plasma - Mass Spectrometer (ICP-MS) was used to measure the concentration of trace elements (NS 4770, 1994 Determination of metals by AAS). The heavy metals (HM) that were chosen for quantitative analysis were chromium (Cr), nickel (Ni), copper (Cu), zinc (Zn), cadmium (Cd), lead (Pb), and mercury (Hg).

The ICP-MS uses electromagnetic induction to ionize the argon atoms and specific metals. The argon atoms are caught in the alternating magnetic field inducing a high intensity energy discharge of 15.8 eV argon ion that creates a plasma torch capable of ionizing most elements on the periodic chart. A metal sample is then introduced as an aerosol to the argon plasma, breaking down the molecular structure of the sample aerosol into atomic gases. The atomic gases are then ionized by the plasma and are guided into, and detected by the mass spectrometer, where each ion is graphed as a trend-line spike assigned to a specified species (Wolf, 2005).

3.7 Micropaleontological analyses

Approximately 5 grams from the homogenized sample was taken out and weighed. The two subsamples were wet-sieved to separate them into different grain size fractions between 63 – 500 μm and > 500 μm. The samples were thoroughly washed with water through a sieve to effectively separating the fractions.

The fine meshed sieve with openings of 63 μm was used to wash away all fecal pellets and other material below the diameter of 63 μm. The two remaining processed fractions were available for analysis. The wet fractionated samples were then transferred into plastic containers and heat dried in a controlled cabinet at 40 °C for 6-8 hours or longer. The dry samples which may have cemented material, were then disintegrated through a 500 μm seive and placed in weighed and labeled glass containers.

The > 500 μm fraction was analyzed to get an overview of sediment contents and presence of foraminifera. For the 63 – 500 μm fraction, a spatula was used to carefully take out minute amounts of material over a picking tray to separate foraminifera adequately. A minimum of approximately 250 foraminiferal samples were picked and placed on a glued faunal slide for counting and species determination. The remaining picked sediments were collected in a glass vial for weighing. The faunal slides were studied, and all species were determined and accounted for.

The foraminifera Norwegian Quality Index (NQI) was calculated to produce the sensitivity index (AMBI) and the diversity index (ES100).

4 Results

Table 4-1 Is a general overview of the marine ecological status of the sediments to establish the water quality based on sample intervals in both cores. The raw data of these samples can be found in appendices (E-G).

Table 4-1: EcoQS classification of biotic indices (Veileder, 2013) and metal concentrations (Veileder, 2016). Foram-AMBI classification (Borja et al 2000) (Alve et al. 2016). TOC % environmental classification (Molvaer et al. 1997). "High" represents reference conditions and shifting towards "Bad" represents very poor conditions (Bouchette, 2018).

EcoQS	High	Good	Moderate	Poor	Bad
Biotic Indices					
NQI	1.0-0.54	0.54-0.45	0.45-0.31	0.31-0.13	0.13-0
ES(100)	35-18	18-13	13-11	11-9	9-0
H'log2	5.0-3.4	3.4-2.4	2.4-1.8	1.8-1.2	1.2-0
AMBI	0.0-1.2	1.2-3.3	3.3-5.0	5.0-6.0	6.0-7
Metals (mg/kg)					
Cadmium	< 0.2	0.2-2.5	2.5-16	16-157	> 157
Lead	< 25	25-150	150-1480	1480-2000	> 2000
Nickel	< 30	30-42	42-271	271-533	> 533
Copper	< 20	20-84	-	84-147	> 147
Zinc	< 90	90-139	139-740	740-6690	> 6690
Chromium	< 60	60-660	660-6000	6000-15500	> 15500
Mercury	< 0.05	0.05-0.52	0.52-0.75	0.75-1.45	> 1.45
TOC (%)	< 2.0	2.0-2.7	2.7-3.4	3.4-4.1	> 4.1

4.1 Sample collection and core description

The JP-19P core replicate reaches 66 cm depth and has a relatively soft and flat surface with little visible sediment suspension. There is visible presence of zooplankton suspended near the surface as well as sixty-one polychaete tubes accounted for, were burrowed into the surface. At 4 to 5 cm interval there is more cohesion of sediment as opposed to fluff. The upper most 5 to 6 cm are green-grey with light brown hints, soft material and the presence of relatively large shells. Traces of bioturbation in the first 8 or 9 cm are present in the green-grey sediment and a hole in the center of the 8 to 9 cm interval. Observation of black striations first appear at 13 to 14 centimeters depth. Very well cohesive sediment by 18 to 19 cm interval. Shells and shell fragments are visible throughout the core shown in figure 4.1.

JP-19Abd sample core reaches 137 cm in depth. The sub-sampling begins at 50cm to avoid excessive overlap between the two cores. The subsamples of the Abdullah core match

characteristics of the gemini core. With initially very dark green silty cohesive sediment down to the bottom of the core (figure 4.1B).

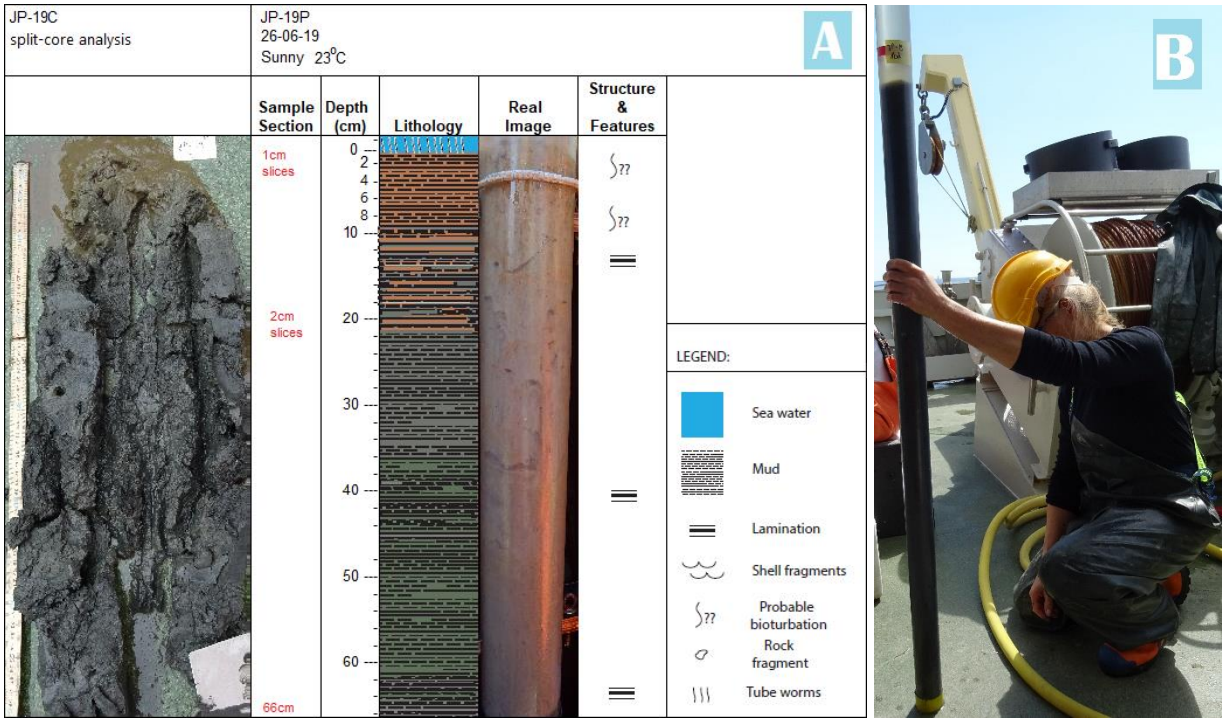

Figure 4.1A-B: A: Replicate split-core JP-19C photo and JP-19P photo with core description. B: Abdullah core JP-19Abd recently retrieved and ready for subsample slicing at the upper deck of Trygve Braarud.

4.2 Water content (WC) and CTD

The JP-19P core sample averages to approximately 60% total WC. Not dropping below 50% in the first 60 cm depth. The first 5 cm depth have increased WC ranging from approximately 76% to 66% due to lacking compaction from the natural sedimentation processes and potential bioturbation disturbances as shown in figures 4.1A and 4.2. The JP-19Abd core sample averages at approximately 45% WC. The cores between Jp-19P and JP-19Abd overlap between 50 and 66 cm. The average between the overlapping portions of the two cores is shown in figure 4.2 and is consistent with the expected trendline. The lowest 5 cm of the Abdullah core has the lowest water content at approximately 41%. The total difference from top of the core JP-19P to the very bottom of JP-19Abd is approximately 35% WC in 137cm.

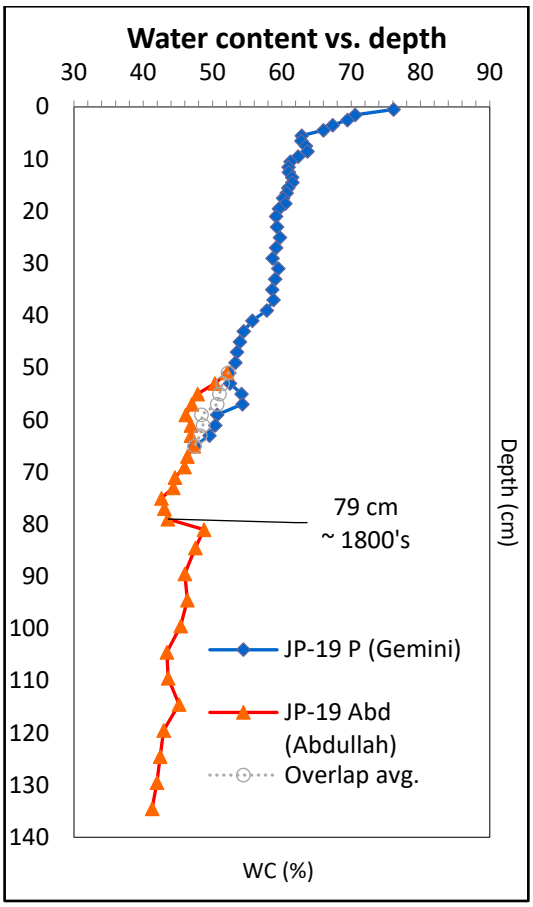

Figure 4.2: Water content percentage of both cores JP-19P and JP-19Abd including average overlap WC. In addition, the 79 cm mark where radioactive isotope dating methods extrapolate approximately around or below the 1800's.

4.3 Grain size analysis

The sediment particulates of station JP-19 are primarily clayey silts (figure 4.3.1), with no particles greater than 270 µm (figure 4.3.2). Average sand content was approximately 4%, with variable lows at 2% from 15cm to 80 cm depths, and peaks > 6% at 6.5 cm and 35 cm depths. There is an increase of sandy sediment at the bottom of the core (134.5 cm) reaching approximately 10%. Silt is the dominant grain size averaging at 55%. Initial depth starts close to the average, and as depth increases, the trend increases as it peaks (61%) at 49 cm depth then continually decreases to the bottom of the core. Clay is the secondary dominant grain size averaging 41% sediments for both cores at station JP-19. Starting relatively low clay content (approx. 38%) and increasing with depth until it peaks at 13.5 cm (approx. 46%). The next two peaks occur in the Abdullah core at 79 and 109.5 cm shown in figure 4.3.1. The upper strata down to approximately 75 cm has more sand and silt relative to clay. Downcore from 75 cm, the clay richness increases seen by the flattening of the bell curve with depth.

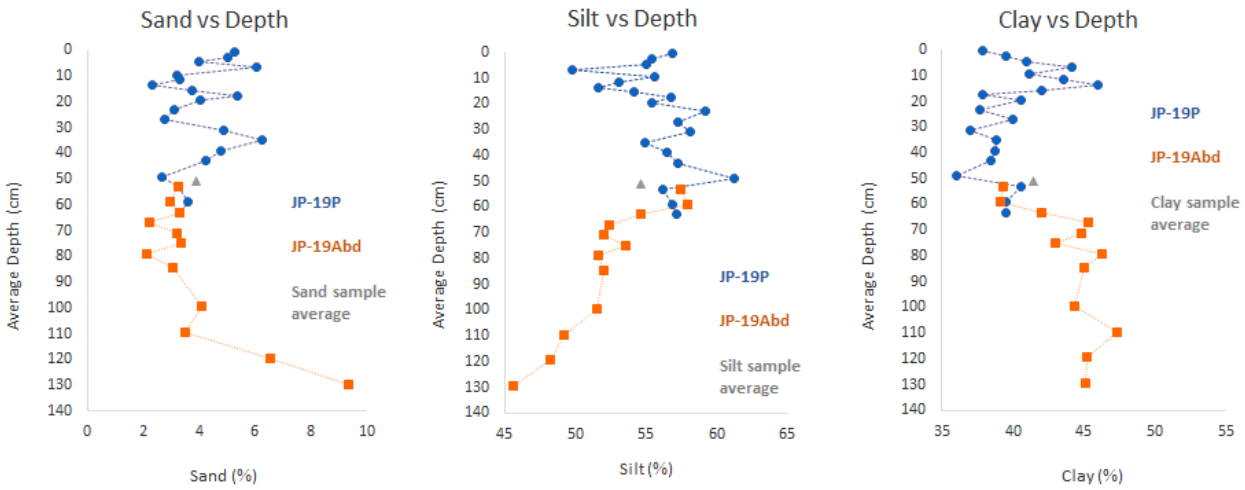

Figure 4.3.1: The three graphs describe sand, silt and clay (%) in relation to depth. The grey triangle in each graph displays the core sample mean based on a 30 sample average that is representative of the entire grain size population of station JP-19.

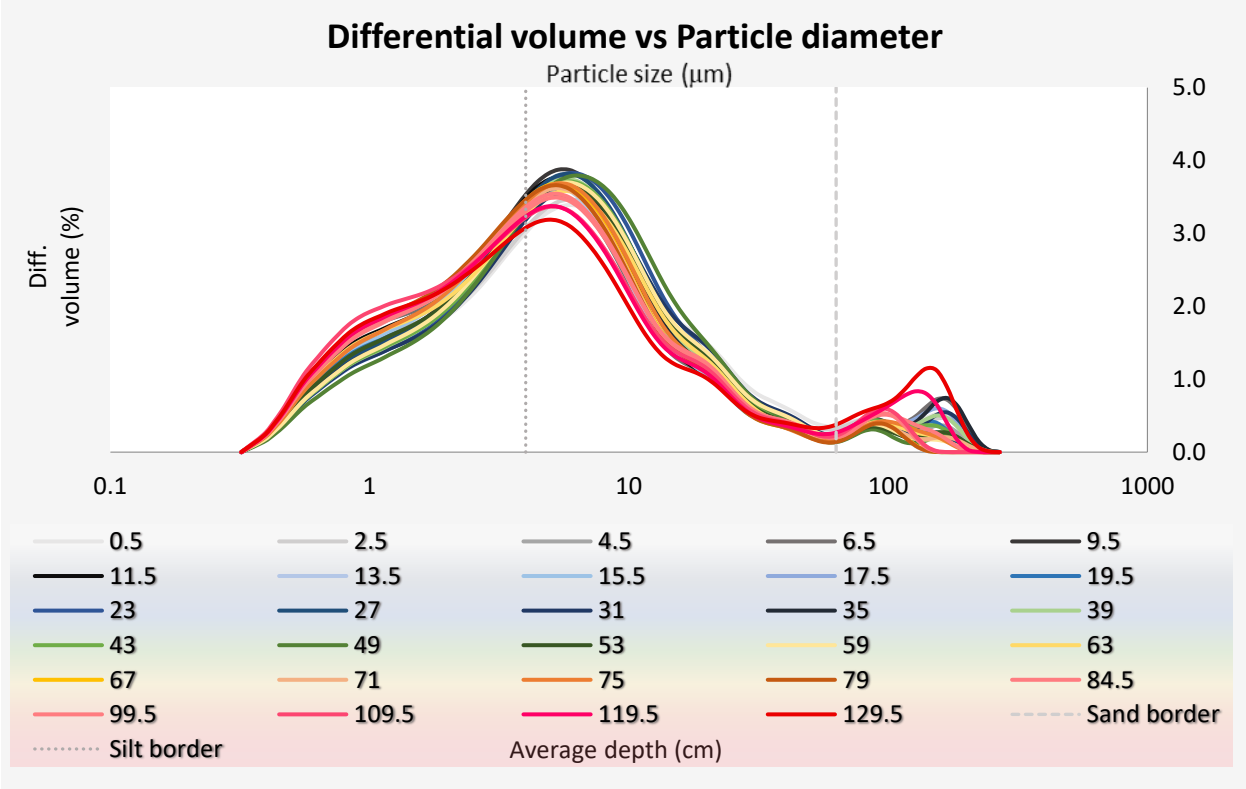

Figure 4.3.2: The upper graph displays a logarithmic scale of differential volume (%) of sediments relative to particle size (µm). The legend below the graph displays the mean depth (cm) and the borders between sand (63 µm) and (silt µm). The graph appears to be 3 dimensional as the cooler colors in the upper depth begin to turn warmer with depth.

4.4 Radio-isotopic dating and sediment accumulation rates (SAR)

The unsupported ^{210}Pb record suggests that sedimentation rate for station JP-19 has not changed

much throughout the entire core, although there is an irregular exponential decline in ^{210}Pb (Bq kg^{-1}). Total and supported ^{210}Pb activity reaches equilibrium with ^{226}Ra at 55 cm where the standard deviation shown in figure 4.4.1 A, reaches up to ± 21 years. The ^{137}Cs radionuclide concentration record shows a sharp peak at 29 cm that seems to strongly support early 1960's atmospheric fallout maximum from nuclear weapons testing. For ^{210}Pb radioactivity CRS model analysis, the year 1963 is dated between 30 and 32 cm. When cross referenced with ^{137}Cs records, a small correction is made to safely match 29 cm with the date 1963.

Sedimentation accumulation rates are at a mean of 0.30 g cm^{-2} y^{-1} between 2019 to 2010 and 0.24 g cm^{-2} y^{-1} from 2010 to 1963 (figure 4.4.1 B). The CRS model with ^{210}Pb records coupled with the ^{137}Cs record give the best estimate in consistent accumulation rates between the early 29 cm (1963) and 42 cm (1935) (Appleby, 2019 - Appendix A).

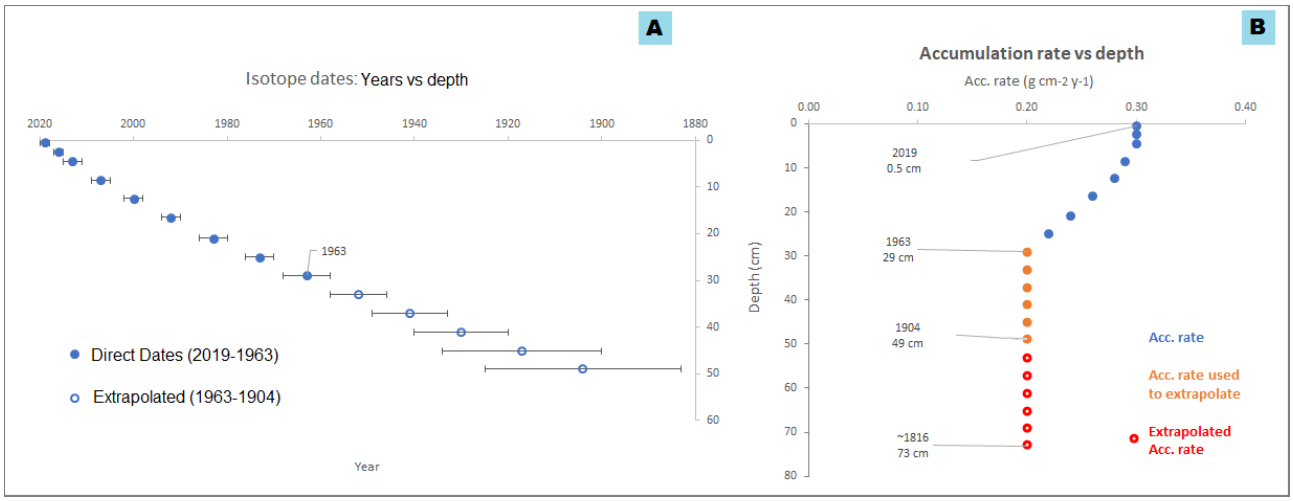

Figure 4.4 A: Dates relative to depth of station JP-19P. Error bars represent the standard deviation in years. **B:** Sediment accumulation rates based on literature by Appleby in Appendix A.

Accumulation rates remain consistent at 0.20 g cm^{-2} y^{-1} for 20 cm (6 samples) downcore from 1963 to 1904. The next 6 samples are linearly extrapolated accumulation rates that reach 24 cm lower into 1816 (figure 4.4.1 B).

4.5 Total organic carbon (TOC) and total nitrogen (TN) content

The following EcoQS of TOC (%) for station JP-19 is described above in Table 4-1. The general trend line for TOC, and TN steadily increases post-19th century until the present date. Starting from the bottom of core JP-19Abd begins in reference conditions up until the turn of the 19th century. From 1904 (49cm) up-core for JP-19P, sediments are in good condition, reaching moderate

conditions at 2.71% at 31 cm depth, representing 1957. Continuing up-core from 31 cm, the EcoQS is in good condition until the top of the core. The depth interval of 4-5 cm dated in 2013 (± 2 years) and 0 – 2 cm interval dated between 2019 to 2018 (± 1 year) are both in moderate condition. The C/N ratios fluctuate in the last decade, as correlated peaks are discernable between TOC, and C/N between the 1952 (± 6 years) and 1941 (± 8 years) with a slight spike in TN. At the overlap between the two cores, The C/N ratio and TOC have a very prominent spike in 59 cm and 63 cm depth.

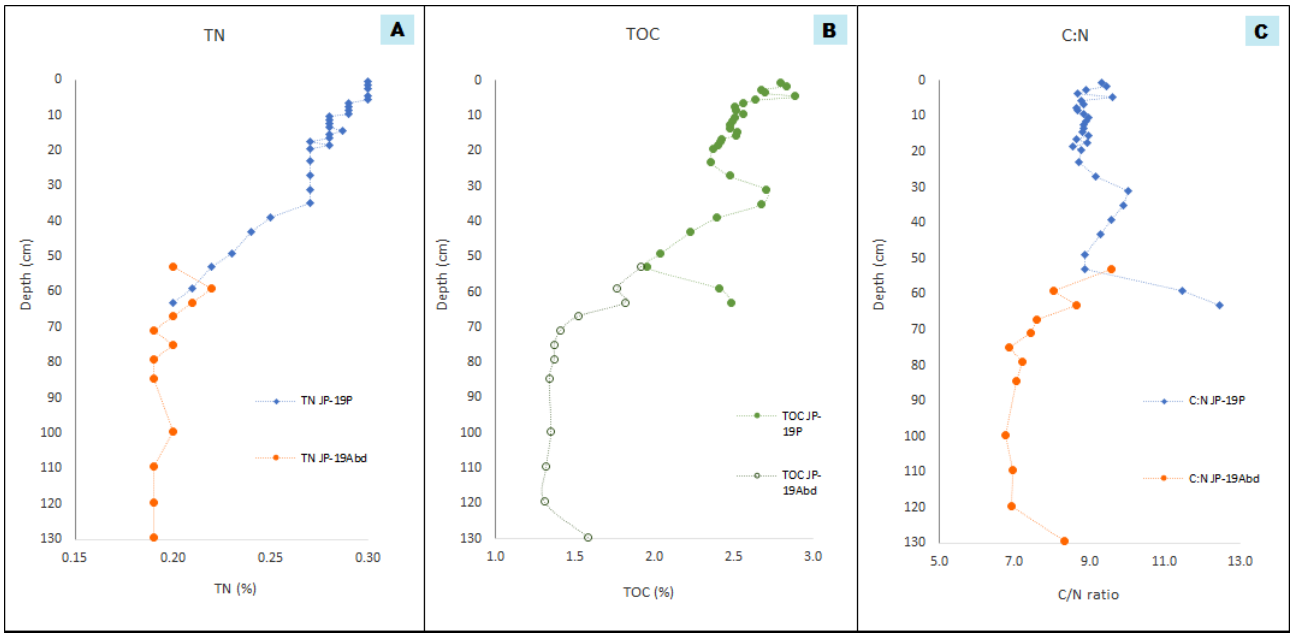

Figure 4.5A-C: A: Represent TN (%) relative to depth. B: Represents TOC (%) concentrations in relation to depth and C: represents the C/N ratio vs. depth.

4.6 Heavy metal (HM) concentrations

Heavy metals at the JP-19 station are predominantly high to good ecological quality (table 4-1) with only two metals dropping as low as moderate. HM fluctuations can all be seen in figure 4.6. The metal concentrations that drop below good EcoQS are Ni and Zn. Nickel is in good quality status throughout the core with only two exceptions where spikes shift the quality to moderate quality only for the JP-19Abd core. One peak is just below the 20th century and the maximum is approximately at the 19the century (figure 4.6). Zinc is moderate throughout most of the core with a prominent peak at approximately 1947 (35 cm). Zinc levels are at good ecological quality throughout the rest of the core and concentrations drop rapidly around 1857, reaching reference conditions around the early 1700's. Zinc, lead, cadmium and mercury all share the same maxima in concentrations at 1947 (± 7 years). Cr and Cd are high EcoQS throughout the core with the record maxima as the only exception of lowering the quality to "good." All HM concentrations peak between the 1970's and 1930's with Ni as the exception. Nickel primarily has little change

throughout the core. Recent values (2010's) for Ni concentrations have comparably to the values in the 19th century and down core.

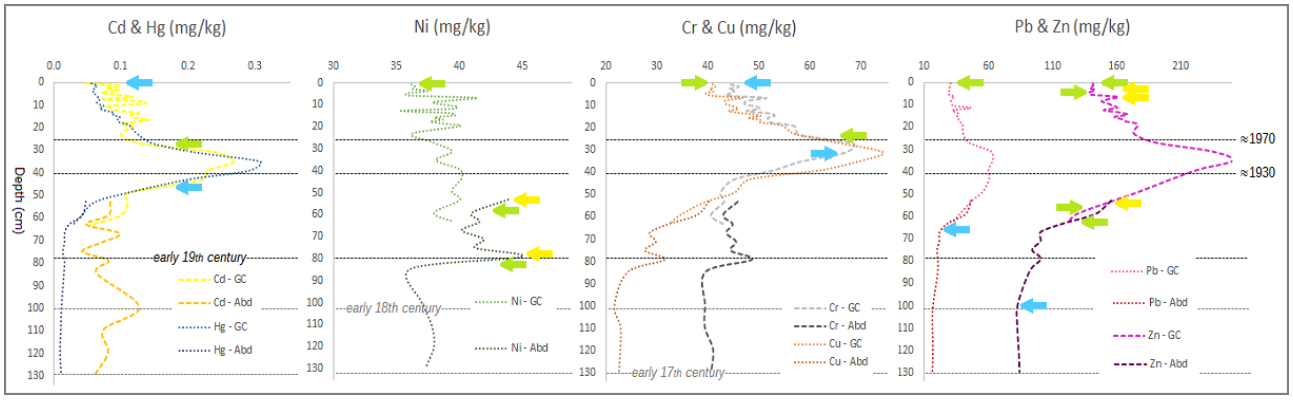

Figure 4.6 Heavy metal concentrations relative to depth. Dashed lines represent recent dates around peaks and the 17th to 19th centuries. Arrows represent changes in EcoQS for Cd, Ni, Cr, Cu, Pb, and Zn (Table 4-1) with depth. The colored arrows pointing at the trend line indicate the initial EcoQS from the surface depth, and the next arrow downcore indicates the point of change in EcoQS. Hg is analyzed semi-quantitatively because the values are below the detectable limit of the ICP-MS and do not accurately represent EcoQS. The ratio between mercury concentrations (mg/kg) still provide an accurate trend in relation to depth.

4.7 Foraminiferal assemblages

The weight of sediments of the greater fractions > 500 µm is negligible for most subsamples, with few foraminifera present. Only two fractions show potential foraminifera content. At 19.5 cm (1985), there seems to be a few large foraminifera and at 39 cm (1935) it is recorded uncertain. At 19.5 cm depth, there is evidence of *Stainforthia fusiformis* and *Uvigerina pelegrinia*. In the 39 cm sample, there is evidence of several *S. fusiformis* and *Nonionella labridorica*, which may have been an error due to contamination from smaller fractions.

Relative abundance of tolerant and opportunistic species, *S. fusiformis* is at a peak in 1985. Sensitive AMBI group *Cassidulina laevigata, Cibicides lobatalus and Hyalinea balthica* are more abundant at around 9.5 cm (2005), in the mid-19th century and in reference conditions.

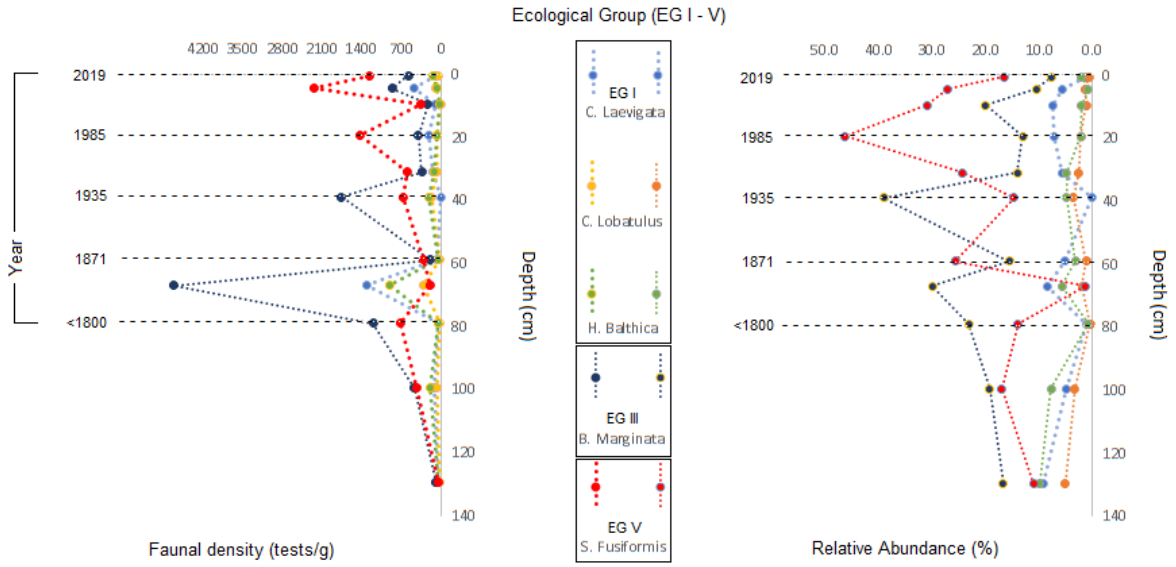

Figure 4.7.1: Two graphs are shown. Faunal density per gram sediments vs. depth – time and relative abundance (%) vs. depth-time. Ecological group classifications: EG I (very sensitive) C to EG V (very resilient).

The foraminifera Norwegian Quality Index (NQI) is calculated to produce the sensitivity index (AMBI) and the diversity indices (ES100, H'log$_2$) shown in figure 4.7.2. The biotic indices indicate a general increase in water quality with all indices returning to "good or high" EcoQS.

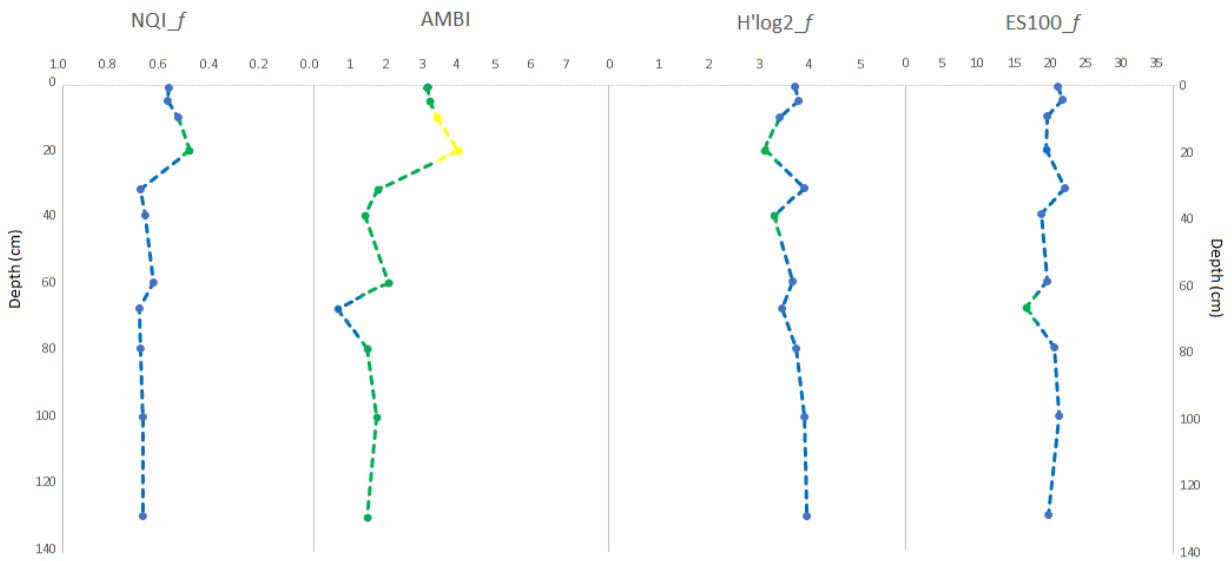

Figure 4.7.2: Biotic indices for foraminifera present for NQI, H'log, ES100 and AMBI. EcoQS colors are represented on the graphs are rake from Table 4-1 above.

Dendogram

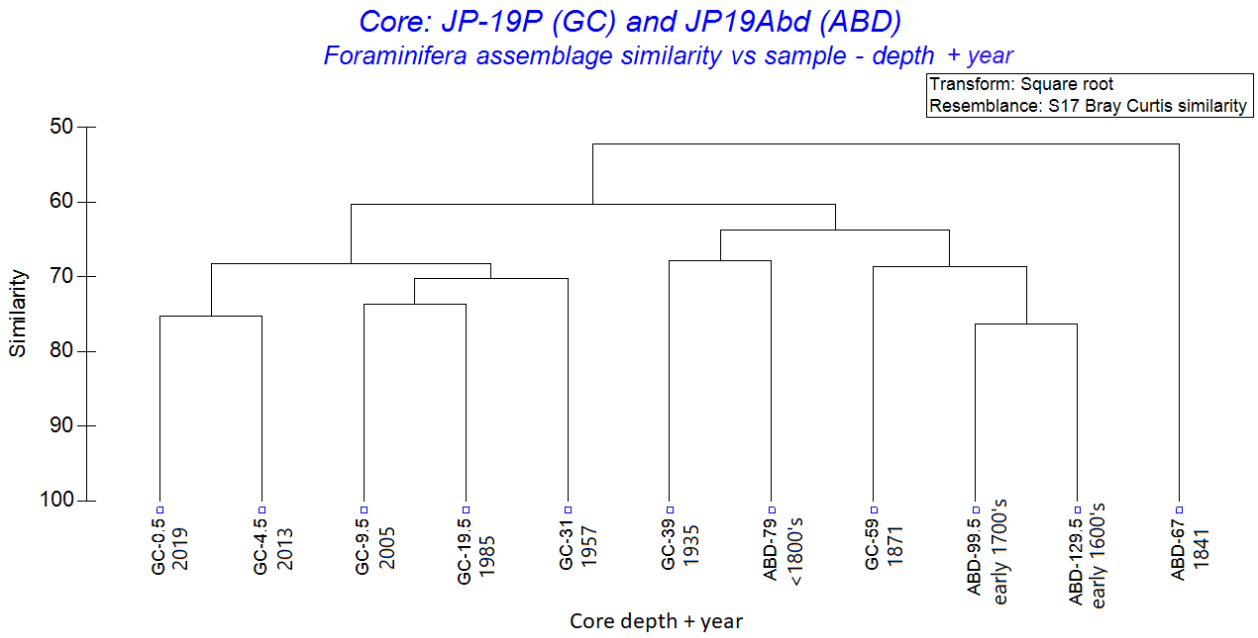

Figure 4.7.3: The Dendrogram is based on Bray Curtis similarity cluster diagram. It represents similarities between foraminifera assemblages relative to depth. The dates are assigned to each depth based on radioisotopes from Appleby, 2019 and interpolated and extrapolated dates.

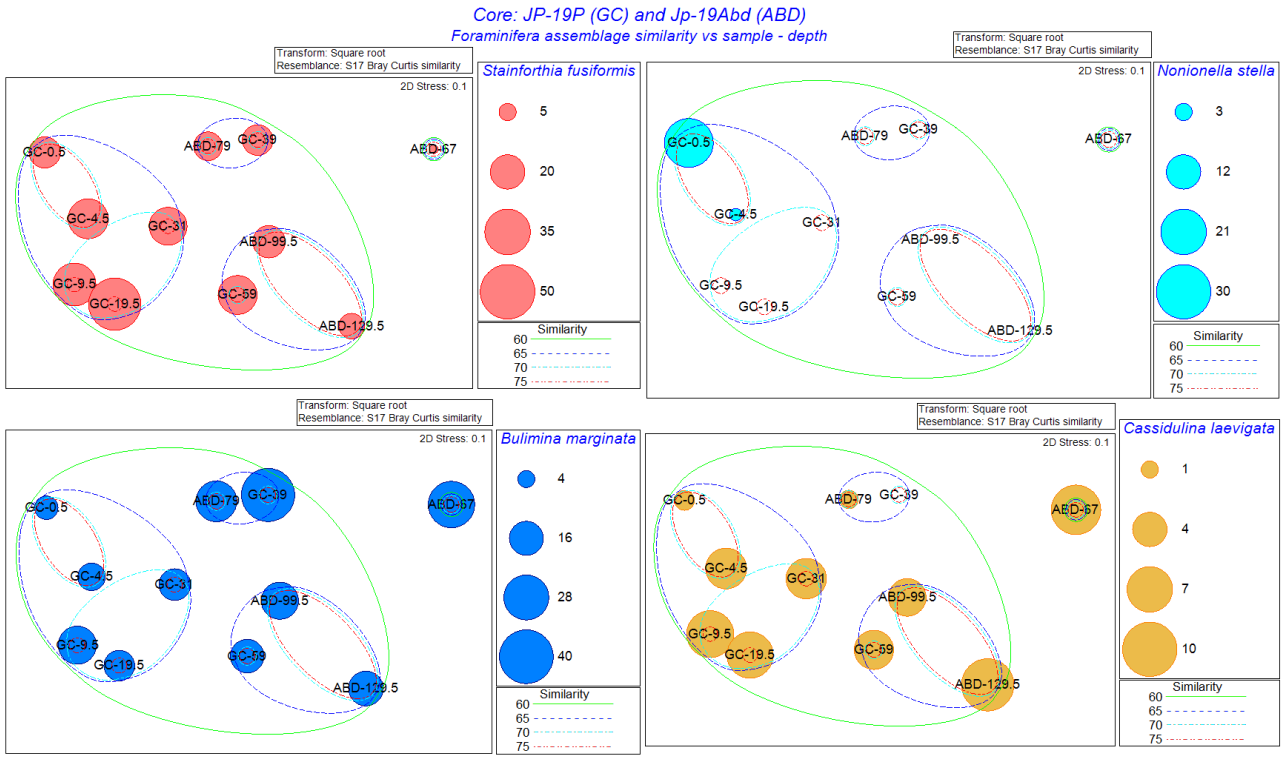

Figure 4.7.4: Multi-dimensional similarity (MDS) plot of benthic foraminifera assemblages from each sample (depth) based on relative abundance data. Assemblages are: C. laevegata (EG I), B. marginata (EG III), S. fusiformis and N. stella (EG V). (N. Stella is competing with Stainforthia and should be placed in an EG 5 (source: Alve - nonionella stella article and Asteman 2015).

5 Discussion

5.1 Sediment Chronology and Depositional environment

The primary contributer in sediment transport in Loperen, Hvaler is the Glomma estuary (Faafeng et al. 1996). WC (%) shows a smooth compaction progression in relation to depth, with what appears to be little disturbances verified by non-oscillatory trends. However, at the overlap between both cores have a contradictory WC record. As JP-19P decreases, JP-19Abd increase at the same level as shown in figure 4.2. This can be due to the presence of bioturbation.
The temporal sedimentation rates at Loperen (Appenidx A) are well over 1 mm per year due to estuarian circulation that it is highly exposed to domestic and industrial effluents following throughout the history of the Glomma river (Hess et al. 2020).

GSA only measured up to 270 μm particle size, when wash and sieved through a > 500 μm mesh during the foraminfera inspection, 3 level had actually shown sediments in that fraction. This can be due to the amount (find number) of material being transferred, is not a precise representative of the general population of grains at the JP-19 station.
The ^{137}Cs artificial radionuclide is caused from atmospheric fallout by nuclear weapons testing that began on a global level in 1953 and reached its peak in 1963 (Appleby, 2001).

Consistent accumulation rates at 0.20 g cm^{-2} y^{-1} provide for extrapolation from 1904 to 1816 as shown in (figure 4.4.1 B). Dating beyond 1904, assuming linear trends of accumulation rates, allowed for dating as far back as the 19th century. If continuing this trend, two more centuries are estimated in figure show in figure 5.1 below.

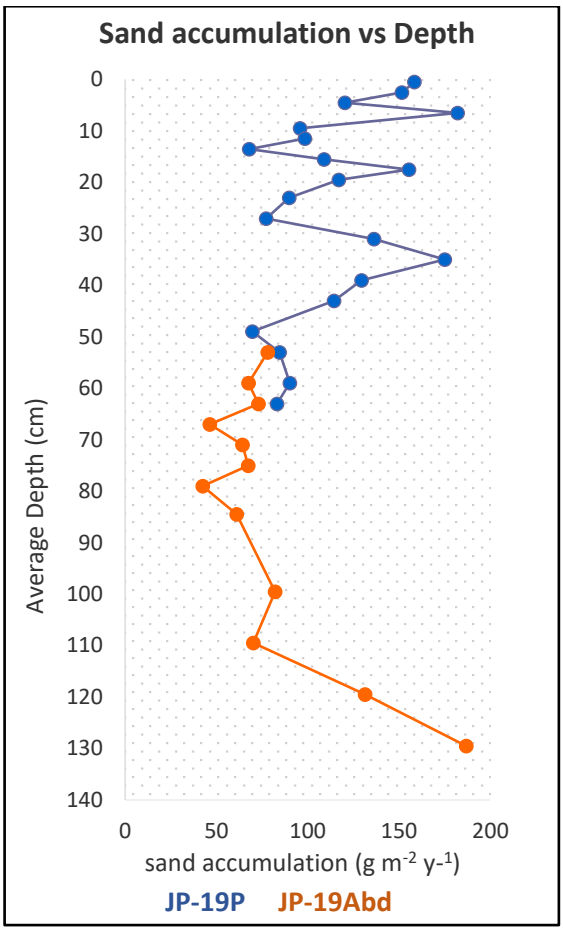

Figure 5.1 Sand sediment accumulation rates (g m^{-2} y^{-1}) relative to depth.

The extrapolated dates down core from the 19th century are less reliable and should be received with caution. The further extrapolations of dates are necessary for visual interpretation of the record during reference conditions. The standard error was large in when reaching sediment depth of 49 cm (1904) (Appleby, 2019), making the extrapolated dates very unreliable. Take the interpretation with caution.

5.2 TOC accumulation rates and HM

The TOC values of station JP-19 begin at reference conditions but increase to moderate conditions in very recent years. Raw data shown in Appendix H. Possibilities of climate change induced melting of ice during the last two winters caused runoff to transport more sediment with carbon traces.

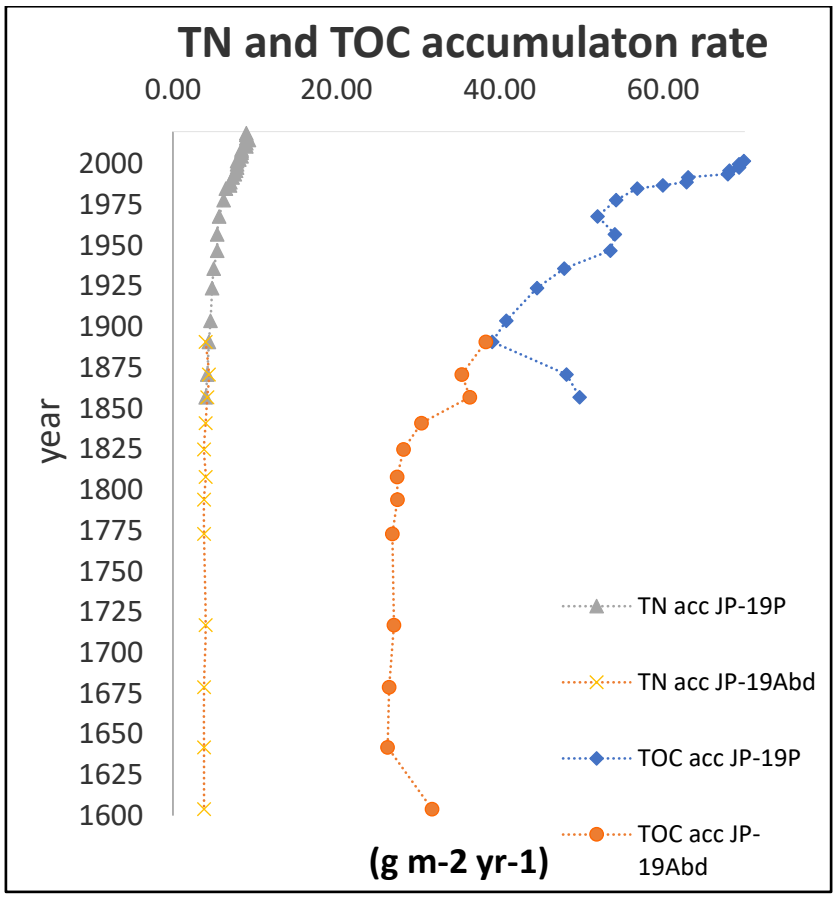

Figure 5.3 Temporal changes of TOC accumulation rates vs depth in relation to TN.

The overlap between both cores at sample depths 59 and 63 cm do not align for TOC, but the trend for TN does not seem unusual. This could imply disturbances at the site due to bioturbation of faunal reworking, burrowing, defecation and general biomixing of sediments (Solan et al. 2019; Kristensen et al. 2014; Dück, 2019).

occurs high peaks around the 1850's - 1890's which are likely to be from lab error based on conflicting information in the sediment record with overlap (the conflict is one decreases a lot, and the other increases). This is evident in disturbances in WC at the overlap making the sediment record at that portion unreliable. This may explain the outliers between the overlap of JP-19P and JP-19Abd between the extrapolated dates 1871 to 1857.

Flash Analyzer for TOC TC TN N could have increased slightly in numbers at the final samples. Running the analyzer will eventually collects material in the tubular chamber that may gradually increase values before replacing the tube. The particle size analyzer was only measured up to 270 µm particle size is not a complete representative of the actual entire grain populations. The weight of all fractions >500 µm was negligible.

HM concentration have the greatest peaks prior to EU mitigation measures (Directive, 2000/60/EC), and have improved in recent years. Cr, Ni and Cd have reached the same concentration as pre-industrial reference conditions. This means that although sediment quality according to Vieleder, 2016 was in "good condition," the concentration levels were still the same in recent years as they were in pre-impacted centuries. Other metals are either good or high quality with no indication of increasing metals concentrations.

The quality status of HM concentrations in sediments, prior to the 19th century, do not reach reference conditions according to Veileder, 2016. This may be due to a minor lab error in measurements, leading to a potential increase in results. Unaccounted for excess of nitric acid may have enhanced results in lower depths.

5.3 Foraminifera assemblages

In the 30 cm fraction > 500 μm, there is evidence of several S. fusiformis and N. labridorica. This is likely due to an error that is determined by the size of the foraminifera in this fraction. The majority are too small and must have been contaminated during the transferring process from the smaller fraction.

Foraminfera EcoQS of diversity indices (ES100, H'log$_2$) are high quality status and only seem to have improved in recent decades. The NQI is also in high quality status and has slightly improved following the trend downcore. There is a slight decrease in quality recently that they are in good to high quality status.

Reinvestigation of samples may be necessary to discover missing data.In the 30 cm fraction > 500 μm, there was evidence of a large number of *S. fusiformis* and *Nonionella labridorica.* This is likely due to an error that is determined by the smaller size of the foraminifera in this larger fraction. The majority of foraminifea in the fraction were too small and must have been contaminants by a smaller fraction during the transferring process in lab.

For subsamples pertaining to foraminifera in the greater than > 500 μm fraction: Formanifera were only found in the 19.5 cm depth subsample. The sample at 67 cm depth may have been unreliable because of inadequate test counts that were significantly lower than other relative samples. The incomplete, or less desirable, foramnifera resolution and further investigation to foraminferal analysis was due to lab shut down for the Covid-19 pandemic.

6 Conclusion

- Temporal TOC accumulation rates have changed from reference conditions to moderate conditions in more recent dates. This may be a sign due to climate change. No strong conclusions were made. Further investigation is necessary to find out why % has increased.

- The Formanifera ecological quality status (EcoQS) of diversity indices are “high” quality status in recent decades. With only AMBI in “good” conditions as of 1985, with up-core trends indicating EcoQS improvement in more recent years.

- Radionuclide signals in JP-19P, had marginally high errors and complicated the result. The irregularities have caused unreliability results for extrapolation below the 19th century. Consider dates with caution.

- Heavy metal (HM) concentrations show evidence of a substantial decrease in recent years.

References

Alve, E. 1996. Benthic foraminiferal evidence of environmental change in the Skagerrak over the past six decades. *Nor. Geol. Unders., Bull.,* 430: 85-93.

Alve, E. 2006. A common opportunistic foraminiferal species as an indicator of rapidly changing conditions in a range of environments. Estuarine, Coastal and Shelf Science 57 (2003) 501–514

Alve, E., Korsun, S., Schönfeld, J., Dijkstra, N., Golikova, E., Hess, S., Husum, K., & Panieri, G. 2016. Foram-AMBI: A sensitivity index based on benthic foraminiferal faunas from North-East Atlantic and Arctic fjords, continental shelves and slopes. *Marine Micropaleontology,* 122: 1-12.

Alve, E., Lepland, A., Magnusson, J. & Backer-Owe, K. 2009. Monitoring strategies for re-establishment of ecological reference conditions: Possibilities and limitations. *Marine Pollution Bulletin,* 59**,** 297-310.

Appleby P.G., & Piliposian, G.T. 2019. Environmental Radioactivity Research Centre: University of Liverpool. Radiometric dating of three marine sediment cores from the Glomma Estuary, Norway. *Revised - January 24, 2020*.

Appleby P.G., 2001. Chronostratigraphic techniques in recent sediments, in *Tracking Environmental Change Using Lake Sediments Volume 1: Basin Analysis, Coring, and Chronological Techniques*, (eds W M Last & J P Smol), Kluwer Academic, pp 171-203.

Appleby, P.G., Nolan, P.J., Gifford, D.W. Godfrey, M.J., Oldfield, F., Anderson, N.J. & Battarbee, R. W. 1986. ^{210}Pb dating by low background gamma counting. *Hydrobiologia* 143, 21–27. https://doi.org/10.1007/BF00026640

Appleby,P.G., Richardson, N. & Nolan, P.J. 1992. Self-absorption corrections for well-type germaniun detectors. *Nucl. Inst.& Methods B*, 71: 228-233.

Arnesen, V. 2001. The pollution and protection of the inner Oslofjord: redefining the goals of wastewater treatment policy in the 20th century. (Special Issue: Man and the Baltic Sea) (Part 2: The Sea and the Cities)(Statistical Data Included). Ambio, 30, 282.

Borja, A., Franco, J., & Perez, V. 2000. A Marine Biotic Index to Establish the Eco logical Quality of Soft-Bottom Benthos Within European Estuarine and Coastal Environments. *Marine Pollution Bulletin,* 40 (12): 1100-1114.

Bouchet, V.M.P., Alve, E., Rygg, B. & Telford, R.J. 2012. Benthic foraminifera provide a promising tool for ecological quality assessment of marine waters. Ecological indicators 2012 v.23 pp. 66-75

Bouchet, V.M.P., Goberville, E. & Frontalini, F. 2018. Benthic foraminifera to assess Ecological Quality Statuses in Italian transitional waters, Ecological Indicators, vol. 84, pp 130-139, ISSN 1470-160X, https://doi.org/10.1016/j.ecolind.2017.07.055.

Borgersen, G. & Walday, M. 2016. Overvåking av Ytre Oslofjord 2014-2018. *Bentosundersøkelser i 2015*. RAPPORT L.NR. no.1788/14

BS EN 13137, 2001. Determination of total organic carbon (TOC) in waste, sludges and sediments.

Bunke, D., Leipe, T., Moros, M., Morys, C., Tauber, F., Virtasalo, J. J., Forster, S., Arz, H. W. 2019. Natural and Anthropogenic Sediment Mixing Processes in the South-Western Baltic Sea. *Front. Mar. Sci. 6:677. doi:10.3389/fmars.2019.00677*

Charm. W. B. 1967. Freeze drying as a rapid method of disaggregating silts and clays for dry particle size analysis. *Journal of Sedimentary Research*; 37 (3): 970–971.

Crossland, C.J., Baird, D., Ducrotoy, J-P., Lindeboom, H., Buddemeier, et al. 2006. The Coastal Zone – a Domain of Global Interactions. Coastal Fluxes in the Anthropocene. pp. 1-23

Directive 2000/60/EC of the European Parliament and of the Council of 23 October 2000 establishing a framework for Community action in the field of water policy. OJ L 327, 22.12.2000, pp 1-51.

Dolven, J. K., Alve, E., Rygg, B. & Magnusson, J. 2013. Defining past ecological status and in situ reference conditions using benthic foraminifera: A case study from the Oslofjord, Norway. *Ecological Indicators,* 29.

Dück, Y., Lorke, A., Jokiel, C. and Gierse, J., 2019. Laboratory and field investigations on freeze and gravity core sampling and assessment of coring disturbances with implications on gas bubble characterization. Limnol Oceanogr Methods, 17: 585-606. doi:10.1002/lom3.10335

Duffield, C. J., Alve, E., Andersen, N., Andersen, T. J., Hess, S., & Strohmeier, T., 2017. Spatial and temporal organic carbon burial along a fjord to coast transect: A case study from Western Norway. *Holocene*, 27 (9), 1325–1339.

Flemming, B. W. and Delafontaine, M. T. 2000. Mass physical properties of muddy intertidal sediments: some applications, misapplications and non-applications. *Cont. Shelf Res.* 20, 1179–1197. doi: 10.1016/S0278-4343(00)00018-2

Faafeng, B., Berge, J. A., Bjerkeng, B., Helland, A., Holtan, G., Holtan, H., Kjellberg, G., Kalqvist, S. T., Moy, F., Kullberg, O. M., Sorensen, K., Walday, M. 1996. “Flommen på Østlandet våren 1995.” Sammenstilling av NIVAs undersøkelser med spesiell vekt på måleprogrammet i Glomma og Vorma. No. 3480

Helland-Hansen, B. and Nansen, F. 1909. The Norwegian Sea. Report on Norwegian Fishery and Marine Investigations. Vol. II, No. 2. Fiskeridirektoratets havforskningsinstitutt.

Helland, A. 2001. The Importance of Selective Transport and Sedimentation in Trend Monitoring of Metals in Sediments. An Example from the Glomma Es tuary, East Norway. Water, Air, & Soil Pollution 126, 339–361. https://doi.org/10.1023/A:1005243728540

Helland, A & Bakke, T. 2002. Transport and sedimentation of Cu in a mi-crotidal estuary, SE Norway. 44(2):149-155. Doi:10.1016/s0025-326x(01)00195-3

Helland, A., Åberg, G. & Skei, J. 2002. Source dependent behaviour of lead and organic matter in the Glomma estuary, SE Norway: evidence from isotope ra tios. Marine Chemistry: *78*(2-3), 149-169. https://doi.org/10.1016/S0304-4203(02)00016-6

Helland, A., Holtan, G. & Jorgensen, P. 2003. Riverine Inputs of Organic Carbon and Nitrogen to Norwegian Coastal Areas. Ambio, Vol. 32, No. 6, pp. 412-417.

Hess, S., Alve, E. & Reuss, N. S. 2014. Benthic foraminiferal recovery in the Oslofjord (Norway): Responses to capping and re-oxygenation. *Estuarine, Coastal and Shelf Science,* 147**,** 87-102.

Holtedahl, H. 1967. Notes on the formation of fjords and fjordvalleys. Geogr Ann 49A:188–203.

IAEA-TECDOC-1360. 2003. Collection and preparation of bottom sediment samples for analysis of radionuclides and trace elements. *International Atomic Energy Agency (IAEA).* ISBN 92–0–109003–X
ISSN 1011–4289

ISO 13320:2009. Particle size analysis — Laser diffraction methods.

Keil, R. 2015. Hoard of fjord carbon. Nature Geosci 8, 426–427. https://doi.org/10.1038/ngeo2433

Kristensen, E., Penha-Lopes, G., Delefosse, M., Valdemarsen, T., Organo Quintana, C. & Banta, G. 2012. What is bioturbation? Need for a precise definition for fauna in aquatic science. Marine Ecology Progress Series. 446. 285-302. 10.3354/meps09506.

Kristiansen, T. & Aas, E. Water type quantification in the Skagerrak, the Kattegat and off the Jutland west coast. Oceanologia. 16. 10.1016/j.oceano.2014.11.002.

Lamb, A. L., Wilson, G. P., & Leng, M. J., 2006. A review of coastal palaeoclimate and relative sealevel reconstructions using δ13C and C/N ratios in organic material. Earth-Science Reviews, 75:1–4, 29–57. https://doi.org/10.1016/J.EARSCIREV.2005.10.003

Lepland, A., Andersen, T.J., Lepland, A., Arp, H.P.H., Alve, E., Breedveld, G.D.,

Rindby, A., 2010. Sedimentation and chronology of heavy metal pollution in Oslo harbor, Norway. *Marine Pollution Bulletin*, 60, 1512–1522.

Lindeboom, H.J. 1995. Protected areas in the North Sea: An absolute need for future marine research. *Helgolander Meeresunters* 49**,** 591–602. https://doi.org/10.1007/BF02368384

Lindeboom H.J. 2002. Changes in Coastal Zone Ecosystems. In: Wefer G., Berger W.H., Behre KE., Jansen E. (eds) Climate Development and History of the North Atlantic Realm. Springer, Berlin, Heidelberg. https://doi.org/10.1007/978-3-662-04965-5_29

Molvaer J, Knutzen J, Magnusson J, Rygg B, Skei J, Sørensen J. 1997. Klassifisering av miljøkvalitet i fjorder og kystfarvann. Veiledning 97:03. SFT TA-1467/1997.

Morton, R., & White, W., 1997. Characteristics of and Corrections for Core Short ening in Unconsolidated Sediments. *Journal of Coastal Research, 13*(3), 761-769. Retrieved August 26, 2020, from http://www.jstor.org/stable/4298671

Murray, J. W., & Alve, E. 2016. Benthic foraminiferal biogeography in NW Euro pean fjords: A baseline for assessing future change. *Estuarine, Coastal and Shelf Science*, *181*, 218–230. https://doi.org/10.1016/J.ECSS.2016.08.014

Naoroz, M., 2018. University of Oslo, Department of Geosciences: Determination of particle size distribution by freeze-drying and Laser analysis of silt and clay. pp 1-2.

Nesje, A. 2009. Fjords of Norway: Complex Origin of a Scenic Landscape. In *Geomorphological Landscapes of the World*. pp. 223-234. Springer Dordrecht.

NS 4770, 1994. Determination of metals by AAS.

Øiestad, V. 1994 Historic changes in cod stocks and cod fisheries: Northeast Arctic cod. ICES mar. Sei. Symp., 198: 17-30.

PN B05577AB. 2011. Laser Diffraction Particle Size Analyzer Manual. *LS 13 320: Laser Diffraction Particle Size Analyzer Instructions for use.* First revision, October 2011.

PUB. 193. 2007. Sailing Directions. Skagerrak and Kattegat. Prepared and published by the National Geospatial-Intelligence Agency. Tenth Edition.

Rygg, B. 1996. Investigations in Hvaler after the great flood in 1995. Soft-bottom fauna and organic material in the sediments. *Norwegian Institute for Water Research (NIWA)*, ISBN No.: ISBN 82-577-3133-1

Ryrfors, T. 2015. Surface circulation in the North-Eastern Skagerrak and the spreading of Glomma water along the Swedish coast. doi:10.13140/RG.2.1.1829.9602.

Schumacher, B. A. 2002 Methods for the determination of total organic carbon (toc) in soils and sediments. United States Environmental Protection Agency, NCEA-C-1282 EMASC-001.

Shoemaker, E.M. 1986. The Formation of Fjord Thresholds. Department of Mathematics, Simon Fraser University, Burnaby, British Columbia V5A lS6, Canada. J*ournal of Glaciology,* Vol. 32, No. 110.

Solan, M., Ward, E.R., White, E.L., Hibberd, E.E., Cassidy, C., Schuster, J.M., Hale, R. and Godbold, J.A. 2019. Worldwide measurements of bioturbation

Staalstrøm, A. & Ghaffari, P. 2015. Current conditions in the Oslofjord: Focus on current strength along the bottom. Report SNO 6799.

Thorsnæs, G. 2015. Store norske leksikon – Løperen.

UiO, 2018. Department of Biosciences: The Faculty of Mathematics and natural sciences website. Research vessel. Description of services – Navigasjonsutstyr, Instrumenter og redskap.

Veileder 02:2013 – revised 2015: Kalssifisering av miljøtilstand i vann – Økologisk og kjemisk klassifieringssystem for kystvann, grunnvann, innsjøer og elver.

Veileder M:608, 2016. Grenseverdier for klassifisering av vann, sediment og biota.

Wintermyer, A.M., Kinter E.B. 1955. Dispersing agents for particles-size analysis of soils. The Physical Research Branch, Bureau of Public Roads. Bull. 95, 1-14.

Wolanski, E. 2007. Estuarine Ecohydrology. Amsterdam: Elsevier. First edition. pp. 1-11. ISBN: 978-0-444-53066-0.

WOLF, R. E., 2005. Ph.D., Research Chemist, USGS/CR/CICT, March 2005. *What is ICP-MS? …and more importantly, what can it do?*

WORMs, 2020. World Register of Marine Species. Retrieved from http://www.marinespecies.org/aphia.php?p=manual. *Accessed: November 2019 – September 2020.*

Appendices

Appendix A: Lab report by radioisotope dating of sediments

Radiometric dating of three marine sediment cores from the Glomma Estuary, Norway

(Revised 24th Jamuary 2020)

P.G.Appleby and G.T.Piliposian
Environmental Radioactivity Research Centre
University of Liverpool

Methods

Dating by ^{210}Pb and ^{137}Cs was carried out on three marine sediment cores from the Glomma Estuary (SE Norway), LS-19, JP-19 and SMA-19. Sub-samples from each core were analysed for ^{210}Pb, ^{226}Ra, and ^{137}Cs by direct gamma assay in the Liverpool University Environmental Radioactivity Laboratory, using Ortec HPGe GWL series well-type coaxial low background intrinsic germanium detectors (Appleby *et al*. 1986). ^{210}Pb was determined via its gamma emissions at 46.5 keV, and ^{226}Ra by the 295 keV and 352 keV γ-rays emitted by its daughter radionuclide ^{214}Pb following 3 weeks storage in sealed containers to allow radioactive equilibration. ^{137}Cs was measured by its emissions at 662 keV. The absolute efficiencies of the detectors were determined using calibrated sources and sediment samples of known activity. Corrections were made for the effect of self-absorption of low energy γ-rays within the sample (Appleby *et al.* 1992).

Results

The results of the radiometric analyses carried out on each core are given in Tables 1–3 and shown graphically in Figures 1.i–3.i. Supported ^{210}Pb activity was assumed to be equal to the measured ^{226}Ra activity, and unsupported ^{210}Pb activity calculated by subtracting supported ^{210}Pb from the measured total ^{210}Pb activity. ^{210}Pb dates were calculated using both the CRS and CIC models (Appleby & Oldfield 1978) where appropriate, and possible 1963 depths determined from the ^{137}Cs record. Best chronologies for each core were determined following an assessment of all the data using the methods outlined in Appleby (2001). The results are shown in Figures 1.ii–3.ii and given in detail in Tables 4–6. Since all three cores had ^{210}Pb inventories well in excess of values supported by the direct atmospheric flux, they all appear to be from sites subject to significant sediment focussing. This process was most intense at the site of core LS-19.

Core LS-19 (Belgen)

Lead-210 Activity

Total ^{210}Pb activity significantly exceeded that of the supporting ^{226}Ra throughout the entire span of the core (Figure 1.i(a)). Unsupported ^{210}Pb concentrations were relatively low and varied irregularly with depth (Figure 1.i(b)). Since values near the base of the core were around 50% of those at the sediment-water interface it appears that the core may span no more than a few decades.

Artificial Fallout Radionuclides

Although ^{137}Cs concentrations (Figure 1.i(c)) also vary irregularly with depth, the general trend is for them to increase steadily with depth. Since highest values are reached near the base of the core, it appears that the entire core (down to a depth of 70 cm) post-dates the period of maximum fallout in the early 1960s.

Core Chronology

Because the core spans only a part of the ^{210}Pb record, dates calculated using the simple CRS model are unlikely to be reliable. They do however suggest a very rapid sedimentation rate, placing 1963 at a depth of around 52 cm. Use of the CIC model is also problematic because of the irregular and non-monotonic fluctuations in the ^{210}Pb concentrations. Disregarding these, the general trend suggests an even more rapid sedimentation rate with 1963 being placed significantly deeper than 70 cm. A reasonable compromise is to suppose that the peak ^{137}Cs concentration in the 64-66 cm dates from the early 1960s. Corrected CRS model dates calculated using this as a reference point suggested a significant acceleration in the sedimentation rate during the past 60 years, from around 0.47 g cm^{-2} y^{-1} (0.84 cm y^{-1}) in the 1960s and 1970s to a mean value of 0.92 g cm^{-2} y^{-1} (1.69 cm y^{-1}) during the past decade. In view of the irregularities in the radiometric records the results, shown in Figure 1.ii and given in detail in Table 4, should however be regarded with some caution unless consistent with other chronological evidence.

Core JP-19 (Løperen)

Lead-210 Activity

Total ^{210}Pb (Figure 2.i(a)) reaches equilibrium with the ^{226}Ra at a depth of around 55 cm. Although the unsupported ^{210}Pb record (Figure 2.i(b)) is again irregular, the more or less exponential decline in concentrations with depth (apart from a section of relatively uniform activity in the uppermost 9 cm) suggests that there has been no major change in the sedimentation rate during the period of time spanned by the core.

Artificial Fallout Radionuclides

The ^{137}Cs activity versus depth record (Figure 2.i(c)) has a well-defined peak between 26-32 cm that almost certainly records the early 1960s fallout maximum from the atmospheric testing of nuclear weapons.

Core Chronology

^{210}Pb dates calculated using the CRS model place 1963 within the 30-32 cm sample, in reasonable agreement with the ^{137}Cs record. Making a small correction to the ^{210}Pb calculations using the 1963 ^{137}Cs date as a reference point, the post-1963 dates are relatively unequivocal. The results suggest a moderate increase in sedimentation rates from a mean value of 0.24 g cm^{-2} y^{-1} (0.47 cm y^{-1}) during the years from 1963-2010 to 0.30 g cm^{-2} y^{-1} (0.71 cm y^{-1}) since then. Irregularities in the ^{210}Pb record below 30 cm make the calculation of reliable pre-1963 dates highly problematic. A best estimate based on the ^{210}Pb record between 29-42 cm suggests that sedimentation rates were comparable to those at the beginning of the 1960s. The results of all these calculations are shown in Figure 2.ii and given in detail in Table 5.

Core SMA-19 (Singlefjord)

Lead-210 Activity

The record in this core is similar to that in JP-19. Total ^{210}Pb (Figure 3.i(a)) reaches equilibrium with the ^{226}Ra at a depth of around 50 cm. Unsupported ^{210}Pb concentrations (Figure 3.i(b)) decline more or less exponentially with depth though there are again a number of significant irregular departures from the general trend.

Artificial Fallout Radionuclides

The ^{137}Cs activity versus depth record (Figure 3.i(c)) has a broad peak between 24-36 cm that almost certainly records the early 1960s fallout maximum from the atmospheric testing of nuclear weapons.

Core Chronology

^{210}Pb dates calculated using the CRS model place 1963 at a depth of around 32 cm, in reasonable agreement with the ^{137}Cs record. The results, shown in Figure 3.ii and given in detail in Table 6, suggest a moderate increase in sedimentation rates since the early 1960s, from a mean value of 0.22 g cm^{-2} y^{-1} (0.50 cm y^{-1}) during the period 1963-2000, to 0.29 g cm^{-2} y^{-1} (0.73 cm y^{-1}) since then. Sedimentation rates prior to 1963 were comparable to those at the beginning of the 1960s, with a mean value of 0.15 g cm^{-2} y^{-1} (0.31 cm y^{-1}).

Extrapolated dates

In this revised report the chronologies given in Tables 4-6 have been extended by assuming that sedimentation rates during earlier times were similar to those during times near the base of the ^{210}Pb record. In LS-19, because of the brevity of the ^{210}Pb record the dates have not been extended beyond the early 1940s. In JP-19 and SMA-19 they have been extended back to the early 19th century. Since extrapolation is an essentially unreliable process these dates should however be regarded with some caution.

References

Appleby P.G., 2001. Chronostratigraphic techniques in recent sediments, in *Tracking Environmental Change Using Lake Sediments Volume 1: Basin Analysis, Coring, and Chronological Techniques*, (eds W M Last & J P Smol), Kluwer Academic, pp171-203.

Appleby,P.G., P.J.Nolan, D.W.Gifford, M.J.Godfrey, F.Oldfield, N.J.Anderson & R.W.Battarbee, 1986. ^{210}Pb dating by low background gamma counting. *Hydrobiologia*, **141**:21-27.

Appleby,P.G. & F.Oldfield, 1978. The calculation of ^{210}Pb dates assuming a constant rate of supply of unsupported ^{210}Pb to the sediment. *Catena*, **5**:1-8

Appleby,P.G., N.Richardson, & P.J.Nolan, 1992. Self-absorption corrections for well-type germaniun detectors. *Nucl. Inst.& Methods B*, **71**: 228-233.

Table 1. Fallout radionuclide concentrations in the Glomma Estuary sediment core LS-19

Depth		^{210}Pb Total		^{210}Pb Unsupported		^{210}Pb Supported		^{137}Cs	
cm	g cm^{-2}	Bq kg^{-1}	±	Bq kg^{-1}	±	Bq kg^{-1}	±	Bq kg^{-1}	±
0.5	0.2	104.9	7.3	72.6	7.4	32.2	1.4	14.4	0.9
2.5	1.3	112.0	6.7	79.0	6.9	33.0	1.5	20.2	1.2
4.5	2.6	108.0	7.4	70.9	7.6	37.2	1.6	15.6	1.1
8.5	4.6	121.3	7.1	82.3	7.3	39.0	1.5	18.7	1.2
12.5	6.8	114.4	7.4	80.7	7.5	33.7	1.4	17.1	1.0
16.5	9.0	111.1	6.1	69.3	6.3	41.8	1.4	19.6	1.1
21.0	11.6	99.3	6.9	58.0	7.1	41.3	1.6	21.1	1.2
25.0	13.9	96.5	5.1	62.0	5.2	34.5	1.1	22.3	0.9
29.0	16.3	112.7	8.1	73.0	8.3	39.6	1.7	22.6	1.3
33.0	18.3	114.0	7.5	78.4	7.7	35.6	1.7	30.1	1.5
37.0	20.7	88.63	7.04	48.6	7.2	40.1	1.5	26.9	1.3
41.0	22.8	90.44	6.96	49.3	7.2	41.1	1.7	24.8	1.3
45.0	24.8	83.3	6.3	47.8	6.5	35.5	1.5	28.0	1.2
49.0	26.8	115.9	9.2	72.1	9.4	43.8	2.1	36.8	1.7
53.0	28.9	95.8	9.9	59.8	10.1	36.0	1.9	31.8	1.6
57.0	31.0	78.2	6.4	44.6	6.6	33.6	1.4	32.6	1.1
61.0	33.3	65.6	5.8	25.6	6.0	40.0	1.4	34.2	1.2
65.0	35.5	81.4	6.2	44.6	6.4	36.8	1.4	44.2	1.3
68.5	37.7	43.3	4.8	10.2	4.9	33.1	1.1	28.8	1.0

Table 2. Fallout radionuclide concentrations in the Glomma Estuary sediment core JP-19

Depth		^{210}Pb Total		^{210}Pb Unsupported		^{210}Pb Supported		^{137}Cs	
cm	g cm^{-2}	Bq kg^{-1}	±	Bq kg^{-1}	±	Bq kg^{-1}	±	Bq kg^{-1}	±
0.5	0.1	165.7	1.0	134.3	11.2	31.4	2.2	17.8	1.6
2.5	0.8	167.0	9.2	134.2	9.4	32.8	2.0	19.0	1.6
4.5	1.6	175.2	9.0	138.7	9.2	36.5	1.8	25.1	1.4
8.5	3.5	169.1	8.7	133.3	8.8	35.9	1.5	30.8	1.5
12.5	5.5	117.8	7.7	82.1	7.9	35.6	1.9	29.1	1.3
16.5	7.6	120.1	6.9	87.7	7.1	32.4	1.6	40.3	1.4
21.0	10.0	92.4	7.5	54.5	7.7	37.9	1.7	56.5	1.6
25.0	12.1	90.5	5.8	52.4	5.9	38.1	1.3	84.7	1.6
29.0	14.3	115.4	9.5	62.2	9.8	53.2	2.1	97.6	2.2
33.0	16.5	71.6	5.5	34.8	5.6	36.8	1.2	36.0	1.1
37.0	18.7	60.8	5.3	25.5	5.5	35.3	1.3	35.6	1.1
41.0	21.0	54.0	4.9	18.1	5.1	35.8	1.3	15.7	0.9
45.0	23.5	64.2	6.1	26.7	6.3	37.4	1.4	8.4	0.8
49.0	26.1	50.6	5.3	15.8	5.4	34.8	1.1	5.0	0.7
53.0	28.8	38.4	4.3	0.8	4.4	37.6	1.1	1.3	0.6
57.0	31.4	37.4	4.8	3.9	4.9	33.5	1.1	1.4	0.6
61.0	34.1	34.5	4.4	-3.0	4.5	37.4	1.0	0.9	0.6

65.0	37.1	29.4	3.2	-7.0	3.4	36.4	1.0	1.4	0.5

Table 3. Fallout radionuclide concentrations in the Glomma Estuary sediment core SMA-19

Depth		^{210}Pb Total		^{210}Pb Unsupported		^{210}Pb Supported		^{137}Cs	
cm	g cm^{-2}	Bq kg^{-1}	±	Bq kg^{-1}	±	Bq kg^{-1}	±	Bq kg^{-1}	±
0.5	0.1	168.6	7.6	133.3	7.8	35.3	1.7	14.1	1.3
2.5	0.8	157.2	0.0	117.0	10.3	40.3	2.2	16.7	1.6
4.5	1.5	136.1	9.6	100.4	9.8	35.8	2.0	20.0	1.4
8.5	3.2	117.3	7.4	82.3	7.5	34.9	1.5	22.2	1.3
12.5	4.9	123.6	7.8	87.1	7.9	36.5	1.6	24.9	1.3
16.5	6.6	84.8	7.5	49.0	7.7	35.9	1.8	26.6	1.5
21.0	8.6	90.3	8.3	57.4	8.5	32.9	1.7	27.7	1.4
25.0	10.3	92.8	7.8	58.6	8.0	34.2	1.6	30.8	1.5
29.0	12.1	76.4	8.0	40.6	8.2	35.8	1.8	30.4	1.5
31.0	13.0	86.3	8.8	50.3	9.0	36.0	2.0	31.7	1.6
33.0	13.9	66.6	7.9	32.9	8.1	33.8	1.9	28.5	1.6
35.0	14.9	65.5	7.7	32.1	7.9	33.5	1.6	29.7	1.5
37.0	15.8	68.9	7.4	35.0	7.6	33.9	1.7	21.0	1.4
41.0	17.8	46.1	5.1	10.4	5.3	35.7	1.3	9.4	0.7
45.0	19.8	54.0	4.9	18.6	5.0	35.5	1.2	3.9	0.8
49.0	21.8	43.0	5.5	7.5	5.7	35.5	1.2	0.5	0.6

Table 4 ^{210}Pb chronology of the Glomma Estuary sediment core LS-19

Depth		Chronology			Sedimentation Rate		
		Date	Age				
cm	g cm^{-2}	AD	y	±	g cm^{-2} y^{-1}	cm y^{-1}	± (%)
0.0	0.0	2019	0	0			
0.5	0.2	2019	0	1	1.05	1.80	10.9
2.5	1.3	2018	1	1	1.01	1.86	9.6
4.5	2.6	2017	2	2	0.95	1.73	11.4
8.5	4.6	2014	5	2	0.90	1.63	9.8
12.5	6.8	2012	7	2	0.89	1.63	10.4
16.5	9.0	2009	10	2	0.87	1.55	10.3
21.0	11.6	2006	13	2	0.84	1.44	13.3
25.0	13.9	2004	15	2	0.76	1.35	10.0
29.0	16.3	2000	19	2	0.69	1.21	12.9
33.0	18.3	1997	22	2	0.66	1.19	11.8
37.0	20.7	1993	26	2	0.64	1.22	16.5
41.0	22.8	1990	29	2	0.61	1.16	16.5
45.0	24.8	1987	32	2	0.52	1.11	16.0
49.0	26.8	1983	36	3	0.47	0.99	11.8
53.0	28.9	1979	40	3	0.47	0.89	11.8
57.0	31.0	1974	45	4	0.47	0.86	11.8
61.0	33.3	1969	50	4	0.47	0.83	11.8

65.0	35.5	1965	54	5	0.47	0.81	11.8
68.5	37.7	1960	59	6	0.47	0.80	11.8
73.0	*40.5*	*1954*	*65*		*0.47*	*0.78*	
77.0	*42.9*	*1949*	*70*		*0.47*	*0.78*	
81.0	*45.3*	*1944*	*75*		*0.47*	*0.78*	

NB: Extrapolated dates are shown in italics

Table 5. ^{210}Pb chronology of the Glomma Estuary sediment core JP-19

Depth		Chronology			Sedimentation Rate		
		Date	Age				
cm	g cm^{-2}	AD	y	±	g cm^{-2} y^{-1}	cm y^{-1}	± (%)
0.0	0.0	2019	0	0			
0.5	0.1	2019	0	1	0.30	0.89	9.4
2.5	0.8	2016	3	1	0.30	0.77	8.3
4.5	1.6	2013	6	2	0.30	0.66	8.2
8.5	3.5	2007	12	2	0.29	0.60	8.6
12.5	5.5	2000	19	2	0.28	0.55	11.5
16.5	7.6	1992	27	2	0.26	0.49	11.1
21.0	10.0	1983	36	3	0.24	0.45	14.6
25.0	12.1	1973	46	3	0.22	0.40	14.6
29.0	14.3	1963	56	5	0.20	0.38	14.6
33.0	16.5	1952	67	6	0.20	0.36	
37.0	18.7	1941	78	8	0.20	0.35	
41.0	21.0	1930	89	10	0.20	0.33	
45.0	23.5	1917	102	17	0.20	0.31	
49.0	26.1	1904	115	21	0.20	0.31	
53.0	*28.8*	*1891*	*128*		*0.20*	*0.30*	
57.0	*31.4*	*1878*	*141*		*0.20*	*0.30*	
61.0	*34.1*	*1864*	*155*		*0.20*	*0.29*	
65.0	*37.1*	*1849*	*170*		*0.20*	*0.29*	
69.0	*40.3*	*1833*	*186*		*0.20*	*0.27*	
73.0	*43.6*	*1816*	*203*		*0.20*	*0.27*	

NB: Extrapolated dates are shown in italics

Table 6. ^{210}Pb chronology of the Glomma Estuary sediment core SMA-19

Depth		Chronology			Sedimentation Rate		
		Date	Age				
cm	g cm^{-2}	AD	y	±	g cm^{-2} y^{-1}	cm y^{-1}	± (%)
0.0	0.0	2019	0	0			
0.5	0.1	2019	0	1	0.29	0.83	7.3
2.5	0.8	2016	3	1	0.29	0.79	9.9
4.5	1.5	2014	5	2	0.29	0.72	10.9
8.5	3.2	2008	11	2	0.29	0.68	10.6
12.5	4.9	2002	17	2	0.29	0.68	10.9

16.5	6.6	1996	23	2	0.26	0.61	13.3
21.0	8.6	1989	30	2	0.24	0.55	12.1
25.0	10.3	1981	38	3	0.22	0.50	15.4
29.0	12.1	1972	47	3	0.19	0.42	15.7
31.0	13.0	1967	52	4	0.17	0.38	21.9
33.0	13.9	1961	58	4	0.15	0.33	13.0
35.0	14.9	1955	64	5	0.15	0.32	13.0
37.0	15.8	1948	71	6	0.15	0.31	13.0
41.0	17.8	1935	84	8	0.15	0.31	13.0
45.0	19.8	1922	97	10	0.15	0.30	13.0
49.0	21.8	1909	110	16	0.15	0.30	13.0
53.0	*23.8*	*1895*	*124*		*0.15*	*0.28*	
57.0	*26.0*	*1881*	*138*		*0.15*	*0.27*	
61.0	*28.3*	*1866*	*153*		*0.15*	*0.27*	
65.0	*30.7*	*1850*	*169*		*0.15*	*0.27*	
69.0	33.1	*1834*	*185*		*0.15*	*0.27*	
73.0	35.6	*1818*	*201*		*0.15*	*0.26*	
77.0	38.0	*1802*	*217*		*0.15*	*0.26*	

NB: Extrapolated dates are shown in italics

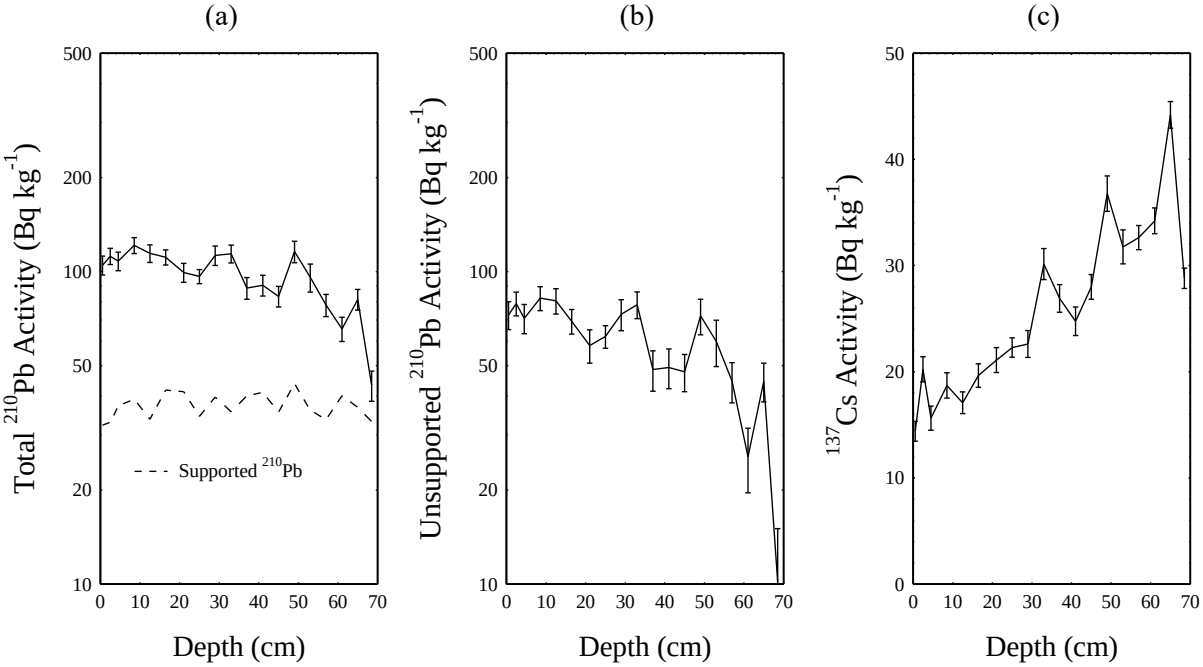

Figure 1.i. Fallout radionuclides in the Glomma Estuary sediment core LS-19 showing (a) total and supported ^{210}Pb, (b) unsupported ^{210}Pb, (c) ^{137}Cs concentrations versus depth.

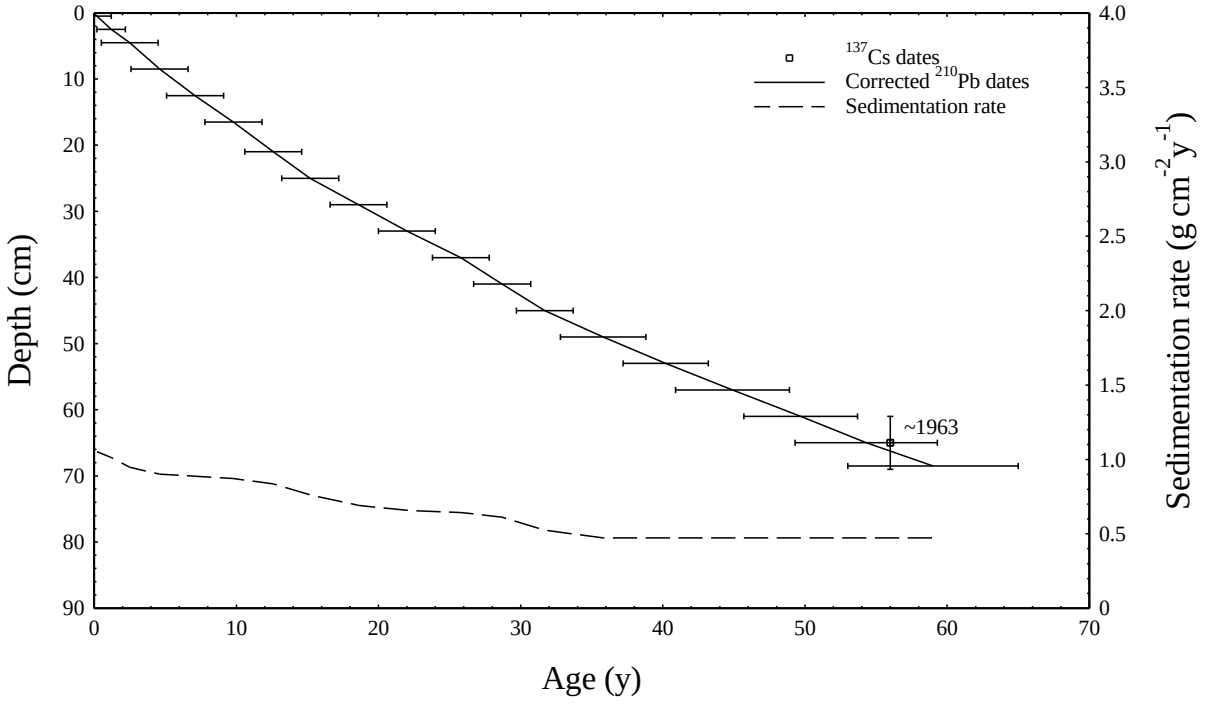

Figure 1.ii. Radiometric chronology of the Glomma Estuary sediment core LS-19 showing the 1963 depth suggested by the ^{137}Cs record and the CRS model ^{210}Pb dates and sedimentation rates calculated using the ^{137}Cs date as a reference point.

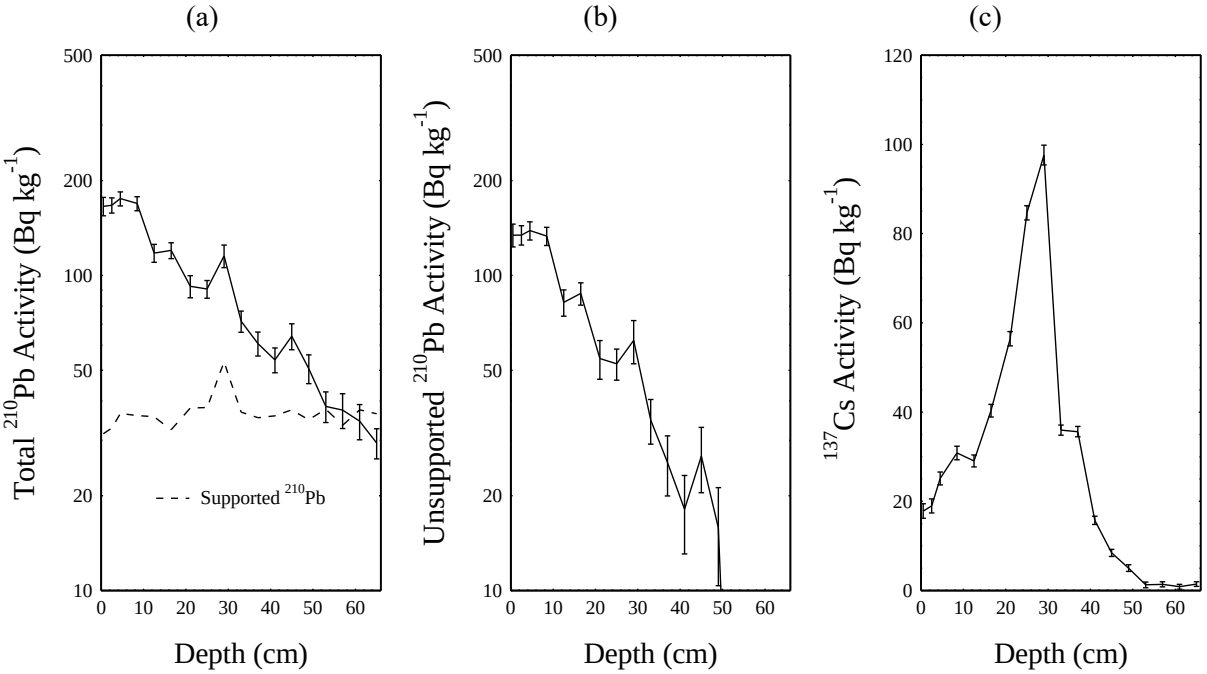

Figure 2.i. Fallout radionuclides in the Glomma Estuary sediment core JP-19 showing (a) total and supported ^{210}Pb, (b) unsupported ^{210}Pb, (c) ^{137}Cs concentrations versus depth.

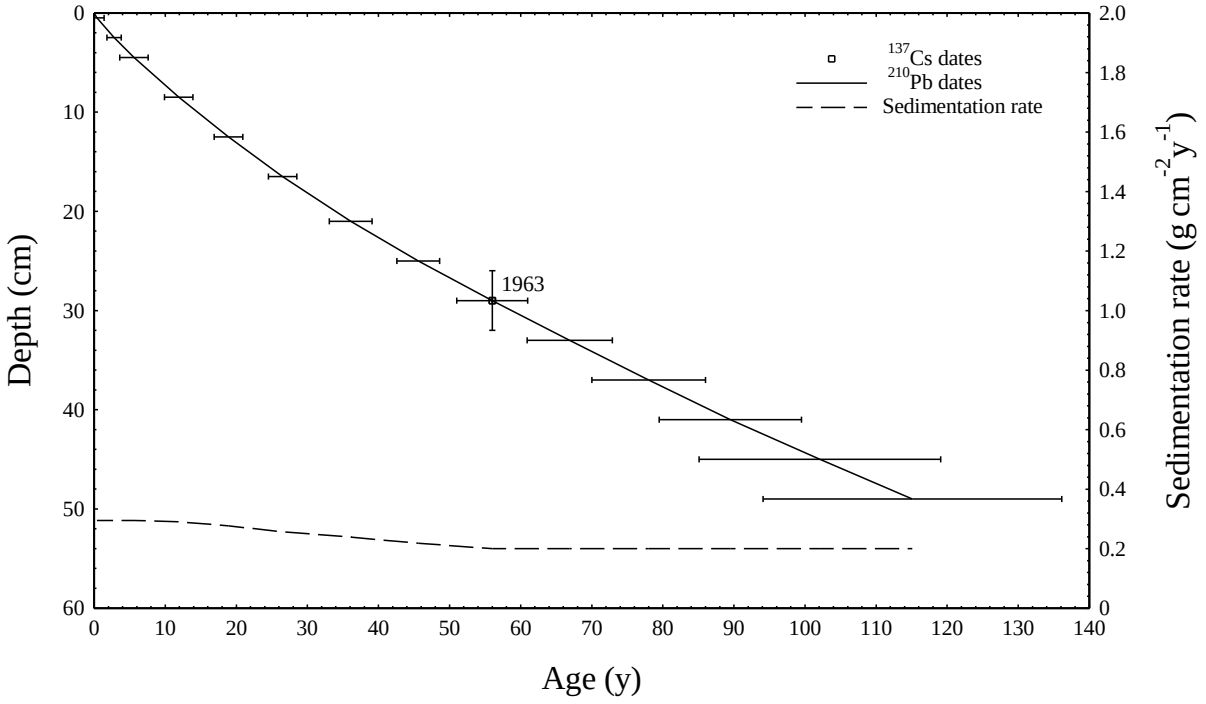

Figure 2.ii. Radiometric chronology of the Glomma Estuary sediment core JP-19 showing the CRS model ^{210}Pb dates and sedimentation rates and the 1963 depth determined from the ^{137}Cs record. A small correction has been made to the ^{210}Pb dates using the ^{137}Cs date as a reference point.

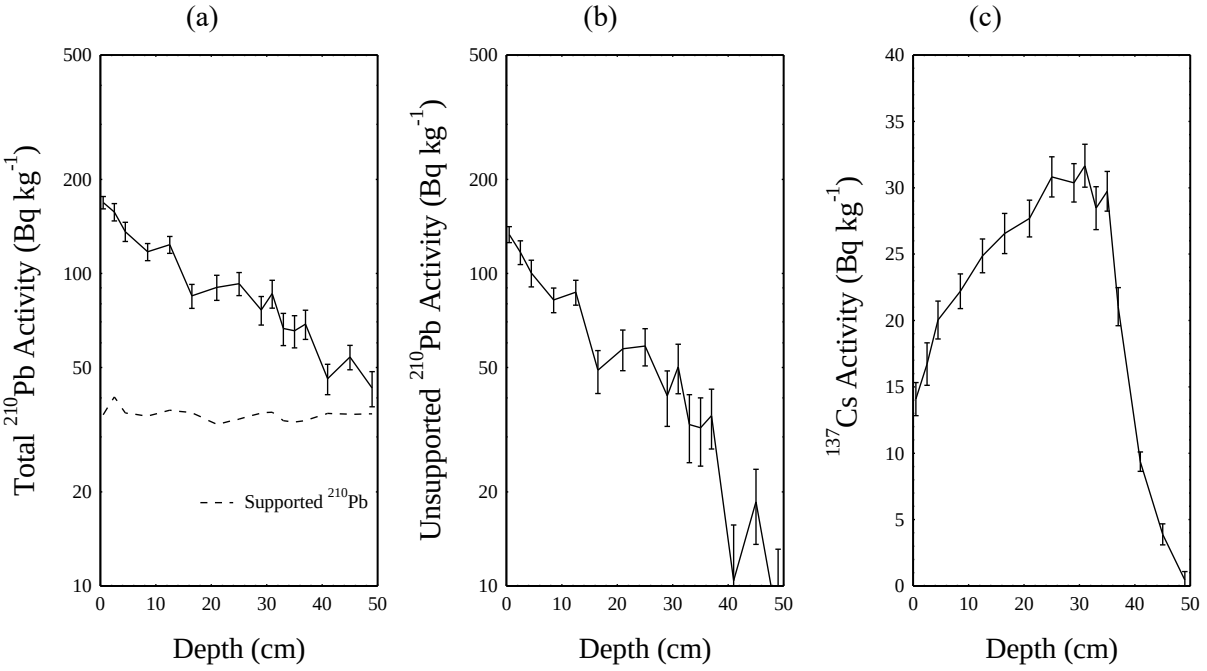

Figure 3.i. Fallout radionuclides in the Glomma Estuary sediment core SMA-19 showing (a) total and supported ^{210}Pb, (b) unsupported ^{210}Pb, (c) ^{137}Cs concentrations versus depth.

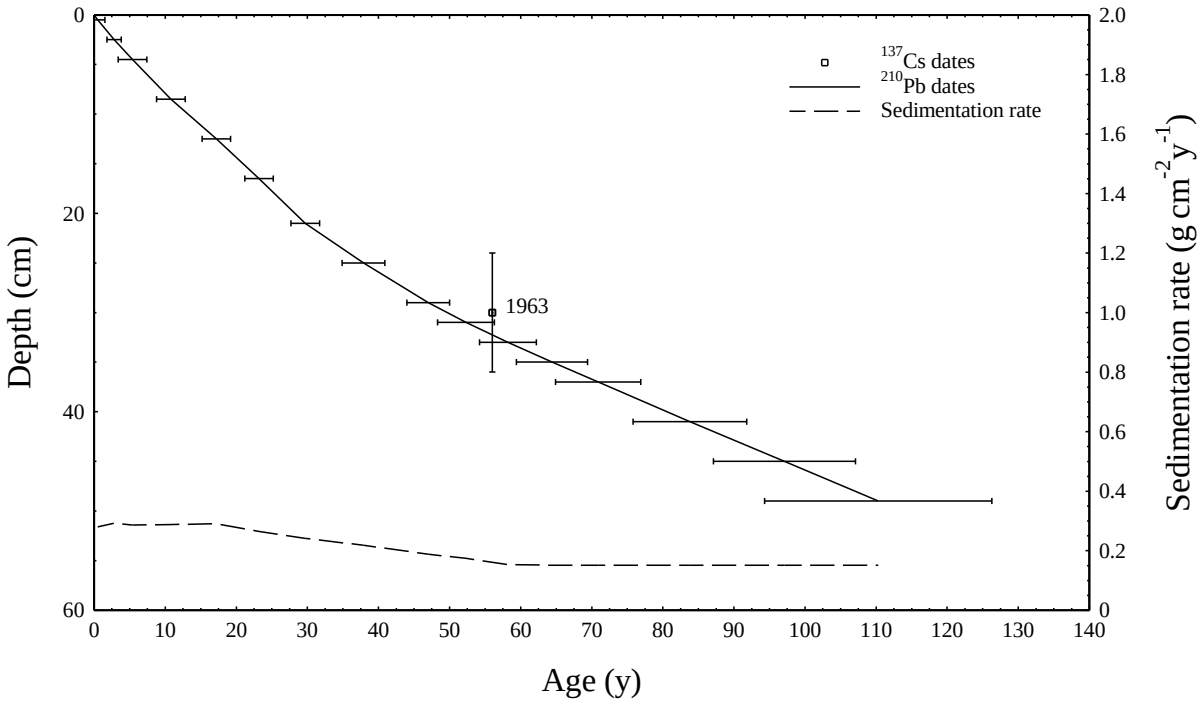

Figure 3.ii. Radiometric chronology of the Glomma Estuary sediment core SMA-19 showing the CRS model ^{210}Pb dates and sedimentation rates and the 1963 depth determined from the ^{137}Cs record.

Appendix B: Core Log of JP-19P

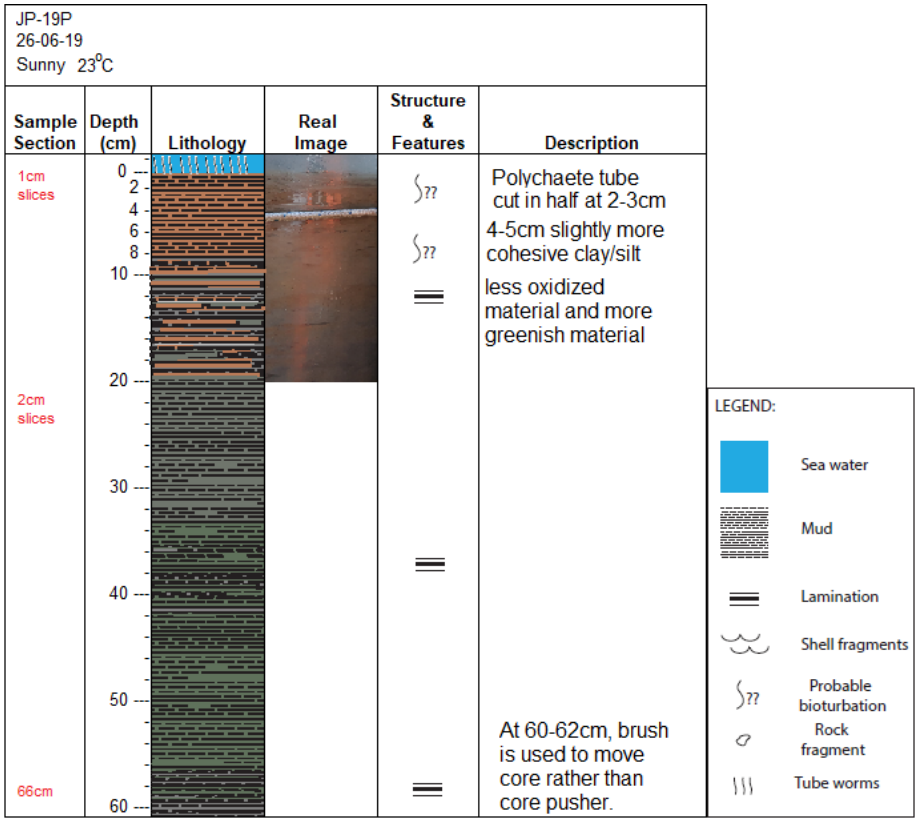

Appendix C: Summary of replicates and samples collected for JP-19 locations 1 and 2.

Sampling Area (old station)	Station Name	Replicate	Equipment	Subsampling (cm)	Sample Treatments	Planned Analysis
Løperen (3SPI)	JP-19	A	CTD, Gemini	2 samples. 0-1 & 1-2 (1 cm ea. Slice)	Rose bengal Staining/ethanol	rB
Løperen (3SPI)	JP-19	B	Gemini	2 samples. 0-1 & 1-2 (1 cm ea. Slice)	Stored in Freezer	TOC & HM
Løperen (3SPI)	JP-19	C	Gemini	vertical core splitting	-	Visual sediment profiile inspection
Løperen (3SPI)	JP-19	D	Gemini	2 samples. 0-1 & 1-2 (1 cm ea. Slice)	Rose bengal Staining/ethanol	rB
Løperen (3SPI)	JP-19	E	Gemini	vertical core splitting	-	Visual sediment profiile inspection
Løperen (3SPI)	JP-19	F	Gemini	2 samples. 0-1 & 1-2 (1 cm ea. Slice)	Rose bengal Staining/ethanol	rB
Løperen (Niwa)	JP-19	G	Gemini	-	-	-
Løperen (Niwa)	JP-19	H	Gemini	vertical core splitting	-	Visual sediment profiile inspection
Løperen (Niwa)	JP-19	I	Gemini	-	-	-
Løperen (Niwa)	JP-19	J	Gemini	-	-	-
Løperen (3SPI)	JP-19	K	Gemini	2 samples. 0-1 & 1-2 (1 cm ea. Slice)	Rose bengal Staining/ethanol	rB
Løperen (3SPI)	JP-19	L	Gemini	2 samples. 0-1 & 1-2 (1 cm ea. Slice)	Stored in Freezer	TOC & HM
Løperen (3SPI)	JP-19	M	Gemini	-	-	-
Løperen (3SPI)	JP-19	N	Gemini	2 samples. 0-1 & 1-2 (1 cm ea. Slice)	Stored in Freezer	TOC & HM
Løperen (3SPI)	JP-19	O	Gemini	-	-	-
Løperen (3SPI)	JP-19	P	Gemini	43 samples 0-20 (1 cm ea.) 20-66 (2 cm ea.)	Stored in Freezer, Freeze drying	TOC & HM, Isotope dating, Foram analysis
Løperen (3SPI)	JP-19	Abd	Abdullah	27 samples 50-82 (2 cm ea. slice) 82-137 (5 cm ea.)	Stored in Freezer, Freeze drying	TOC & HM, Isotope dating, Foram analysis
Løperen (3SPI)	JP-19	I	Grab Sampler	0.1 m^2 suface area	Stored in Large container for bio specimen	Biology lab
Løperen (3SPI)	JP-19	II	Grab Sampler	0.1 m^2 suface area	Stored in Large container for bio specimen	Biology lab
Løperen (3SPI)	JP-19	III	Grab Sampler	0.1 m^2 suface area	Stored in Large container for bio specimen	Biology lab

Appendix D: Sample Overview of cores: JP-19P & JP-19Abd

Box No.	Core in-terval depth (cm)	core depth av. (cm)	Forams	GSA (grain)	Metal	TC	TOC	TN	Radio isotope Dates
1	0-1	0.5	x	2x	x	x	x	x	x
2	1-2	1.5			x	x	x	x	
3	2-3	2.5		2x	x	x	x	x	x
4	3-4	3.5			x	x	x	x	
5	4-5	4.5	x	2x	x	x	x	x	x
6	5-6	5.5			x	x	x	x	
7	6-7	6.5		2x	x	x	x	x	
8	7-8	7.5			x	x	x	x	
9	8-9	8.5			x	x	x	x	x
10	9-10	9.5	x	2x	x	x	x	x	
11	10-11	10.5			x	x	x	x	
12	11-12	11.5		2x	x	x	x	x	
13	12-13	12.5			x	x	x	x	x
14	13-14	13.5		2x	x	x	x	x	
15	14-15	14.5			x	3x	3x	3x	
16	15-16	15.5		2x	x	x	x	x	
17	16-17	16.5			x	x	x	x	x
18	17-18	17.5		2x	x	x	x	x	
19	18-19	18.5			x	x	x	x	
20	19-20	19.5	x	2x	x	x	x	x	
21	20-22	21							x
22	22-24	23		2x	x	x	x	x	
23	24-26	25							x
24	26-28	27		2x	x	x	x	x	
25	28-30	29							x
26	30-32	31	x	2x	x	x	x	x	
27	32-34	33							x
28	34-36	35		2x	x	x	x	x	
29	36-38	37							x
30	38-40	39	x	2x	x	x	x	x	
31	40-42	41							x
32	42-44	43		2x	x	x	x	x	
33	44-46	45							x
34	46-48	47							
35	48-50	49		2x	x	x	x	x	x
36	50-52	51							
37	52-54	53		2x	x	x	x	x	*0*
38	54-56	55							
39	56-58	57							*0*
40	58-60	59	x	2x	x	x	x	x	
41	60-62	61							*0*
42	62-64	63		2x	x	3x	3x	3x	

43	64-66	65							*0*
Abdul-lah	Overlap								
44	50-52	51							
45	52-54	53		2x	x	x	x	x	*0*
46	54-56	55							
47	56-58	57							*0*
48	58-60	59		2x	x	x	x	x	
49	60-62	61							*0*
50	62-64	63		2x	x	x	x	x	
51	64-66	65							*0*
52	66-68	67	o	2x	x	x	x	x	
53	68-70	69							*0*
54	70-72	71		2x	x	x	x	x	
55	72-74	73							*0*
56	74-76	75		2x	x	x	x	x	
57	76-78	77							
58	78-80	79	x	2x	x	x	x	x	
59	80-82	81							
60	82-87	84.5		2x	x	x	x	x	
61	87-92	89.5							
62	92-97	94.5							
63	97-102	99.5	x	2x	x	x	x	x	
64	102-107	104.5							
65	107-112	109.5		2x	x	x	x	x	
66	112-117	114.5							
67	117-122	119.5		2x	x	x	x	x	
68	122-127	124.5							
69	127-132	129.5	x	2x	x	3x	3x	3x	
70	132-137	134.5							

x = complete samples

o/*0* = incomplete sample/*extrapolated results*

number next to "x" = number of replicates

Abdul-lah	Overlap between cores JP-19P and JP-19Abd

Appendix E: Metal Concentrations Lab Report and dates

Box#	depth	Dates	Cr (ppb)	%RSD	Ni (ppb)	%RSD	Cu (ppb)	%RSD
M1	0.5	**2019**	44.56	4.58	36.42	2.52	41.13	0.84
M2	1.5	*2018*	49.44	3.56	39.23	0.49	44.54	1.07
M3	2.5	**2016**	48.22	2.72	39.77	2.07	44.12	2.09
M4	3.5	*2015*	51.68	3.61	42.93	4.62	47.05	3.04
M5	4.5	**2013**	51.54	1.60	41.73	0.45	46.07	1.44
M6	5.5	*2011*	53.02	1.69	43.68	1.26	49.32	2.67
M7	6.5	*2009*	53.58	5.78	43.15	4.40	48.85	2.80

M8	7.5	*2008*	50.47	2.19	41.65	6.44	45.41	4.01
M9	8.5	**2007**	49.52	2.26	39.91	1.73	45.44	0.90
M10	9.5	*2005*	50.16	2.80	40.88	1.82	46.22	1.38
M11	10.5	*2003*	53.75	2.40	43.28	1.60	49.03	2.60
M12	11.5	*2002*	50.54	1.39	40.10	1.86	46.37	1.18
M13	12.5	**2000**	54.12	2.22	40.35	3.53	50.20	2.89
M14	13.5	*1998*	55.64	2.06	41.85	0.83	50.35	1.66
M15	14.5	*1996*	54.34	4.21	40.69	2.64	51.55	3.55
M16	15.5	*1994*	59.72	1.52	44.04	2.68	55.25	1.09
M17	16.5	**1992**	55.66	1.85	41.38	1.43	53.96	1.36
M18	17.5	*1989*	53.73	1.57	38.84	1.69	51.77	1.13
M19	18.5	*1987*	57.35	1.41	40.54	1.75	55.83	4.28
M20	19.5	*1985*	63.56	2.85	44.51	2.42	61.18	2.00
M22	23	*1978*	69.17	1.97	43.40	2.80	68.69	1.51
M24	27	*1968*	76.59	2.52	42.52	1.92	74.23	1.71
M26	31	*1957*	65.16	2.06	38.40	2.91	72.35	1.13
M28	35	1947	63.43	1.95	41.50	1.72	75.52	1.93
M30	39	1936	53.74	1.77	40.75	1.05	63.07	0.98
M32	43	1924	47.40	1.06	42.23	1.20	50.61	1.27
M35	49	*1904*	45.97	3.23	42.75	3.77	49.02	1.86
M37	53	**1891*	46.86	2.49	43.54	1.62	43.06	1.00
M40	59	**1871*	46.49	2.82	43.66	2.62	39.67	2.31
M42	63	**1857*	44.76	1.36	41.33	1.58	33.97	0.70
M45	53	**1891*	46.13	3.81	44.17	1.77	40.36	1.23
M48	59	**1871*	46.41	3.43	44.30	1.19	40.79	1.97
M50	63	**1857*	48.50	1.96	45.04	1.65	34.90	0.87
M52	67	**1841*	50.03	3.02	46.17	1.41	32.80	2.00
M54	71	**1825*	47.63	1.11	43.92	2.55	31.16	1.63
M56	75	~**1808*	49.26	1.83	45.78	1.87	30.60	2.17
M58	79		52.11	1.76	48.25	1.35	33.80	2.07
M60	84.5		47.46	2.44	43.42	1.98	29.19	0.83
M63	99.5		42.08	1.62	39.48	1.69	23.17	1.69
M65	109.5		44.07	2.24	42.27	1.64	25.61	3.34
M67	119.5		49.79	1.89	46.15	1.20	27.73	1.11
M69	129.5		44.78	3.37	41.16	0.96	24.85	2.87

Date: Bold is directly dated, *italic* is interpolated, *asterik is extrapolated

Standards run as unknowns								
Blank	0.02	174.50	0.02	174.50	-0.02	115.70	-0.04	183.80
TMDW	20.48	4.23	20.48	4.23	62.07	1.55	20.46	3.72
TMDW	21.83	5.27	21.83	5.27	65.22	3.19	21.58	2.58
6020-100ppb	117.66	1.44	117.66	1.44	121.06	0.64	109.38	0.45
Detection limit of method								
	0.07		0.07		0.07		0.11	
Semi-quantitative analysis								

	Zn (ppb)	**%RSD**	**Cd (ppb)**	**%RSD**	**Hg (ppb)**	**%RSD**	**Pb (ppb)**	**%RSD**

M1	142.25	1.58	0.05	94.02	1.11	12.96	30.70	1.11
M2	152.38	1.32	0.11	52.21	1.34	7.83	32.94	0.36
M3	152.14	1.47	0.08	38.44	1.19	5.58	32.27	1.23
M4	164.25	3.09	0.11	39.81	1.28	15.14	34.07	3.28
M5	161.53	1.51	0.08	47.29	1.21	15.96	33.48	0.28
M6	169.40	1.39	0.11	48.64	1.36	16.09	35.48	1.90
M7	168.33	3.15	0.12	60.07	1.24	10.78	34.95	3.08
M8	160.78	4.34	0.08	40.87	1.31	9.14	32.63	4.08
M9	155.97	1.34	0.14	20.44	1.29	7.50	32.32	1.19
M10	162.52	1.81	0.14	48.16	1.31	10.52	33.40	0.92
M11	170.88	1.61	0.08	46.32	1.48	4.01	35.15	0.38
M12	162.08	1.94	0.09	74.06	1.37	10.88	47.06	0.61
M13	170.88	2.34	0.10	33.66	1.68	10.64	36.66	1.35
M14	172.92	1.01	0.13	31.34	1.80	16.76	37.85	1.00
M15	172.78	2.52	0.12	37.87	1.77	4.24	37.79	2.37
M16	183.30	2.39	0.13	42.19	2.06	10.10	40.96	0.48
M17	175.32	1.81	0.15	18.18	1.90	3.49	39.17	0.82
M18	171.97	2.12	0.12	31.09	2.01	7.51	38.11	0.71
M19	182.62	2.50	0.11	24.89	2.17	8.65	41.45	1.19
M20	196.40	2.04	0.13	50.17	2.38	3.94	44.54	0.64
M22	207.98	1.24	0.12	23.76	2.59	5.57	48.37	1.16
M24	212.87	2.15	0.14	38.78	3.18	6.26	49.95	0.59
M26	228.49	0.76	0.24	23.86	4.17	7.27	60.48	0.60
M28	273.20	1.90	0.29	18.33	6.30	8.14	69.03	0.61
M30	228.81	1.91	0.23	24.98	5.83	3.16	61.20	0.79
M32	214.96	1.13	0.23	21.64	3.99	5.83	63.85	0.68
M35	192.81	1.38	0.12	64.92	2.25	9.82	60.69	1.00
M37	171.64	0.95	0.12	61.36	1.26	11.72	51.64	0.87
M40	148.34	1.91	0.11	42.90	0.85	16.21	43.34	0.42
M42	127.28	1.33	0.06	58.34	0.55	18.96	33.34	0.28
M45	156.70	0.70	0.08	46.64	0.91	17.95	46.94	0.21
M48	154.73	1.26	0.09	51.95	0.87	17.60	45.61	0.66
M50	129.33	0.81	0.05	37.10	0.45	19.48	30.88	0.93
M52	115.89	1.95	0.11	53.75	0.33	31.94	25.07	0.38
M54	105.80	1.73	0.07	46.57	0.31	21.19	22.76	1.35
M56	104.70	1.27	0.05	133.70	0.27	27.44	21.96	0.55
M58	108.56	3.17	0.09	39.01	0.31	23.37	21.86	0.45
M60	111.00	1.61	0.08	54.07	0.31	21.34	24.54	0.55
M63	88.76	2.71	0.14	8.83	0.23	51.02	17.82	1.01
M65	92.74	2.18	0.08	63.96	0.20	12.47	18.06	1.42
M67	101.88	2.13	0.10	53.55	0.19	19.13	20.11	1.00
M69	93.31	1.92	0.07	25.52	0.21	26.10	17.75	1.22
Standards run as unknowns								
Blank	-0.12	101.00	0.00	-	0.08	54.84	-0.05	122.60
TMDW	75.22	5.21	10.75	7.29	0.17	32.98	21.08	1.19
TMDW	79.38	2.39	10.09	4.14	0.10	44.78	19.94	1.24

6020-100ppb	107.90	1.11	99.93	1.49	0.06	41.12	98.57	0.33
Detection limit of method								
	0.19		0.02		0.06		0.13	
Semi-quantitative analysis								

Appendix F: Metal concentrations & dates (direct, interpolated and extrapolated)

Metal concentrations and dates:

av.depth	Cr (ppm)	Ni (ppm)	Cu (ppm)	Zn (ppm)	Cd (ppm)	Hg (ppm)	Pb (ppm)	Dates	Acc. Rate (g cm-2 y-1)
0.5	44.30	36.21	40.89	141.42	0.047	0.056	30.52	**2019**	**0.30**
1.5	46.00	36.49	41.43	141.76	0.098	0.065	30.64	*2018*	
2.5	44.04	36.33	40.30	138.97	0.077	0.059	29.48	**2016**	**0.30**
3.5	45.10	37.47	41.06	143.33	0.097	0.061	29.73	*2015*	
4.5	44.22	35.79	39.53	138.57	0.071	0.058	28.72	**2013**	**0.30**
5.5	43.48	35.82	40.44	138.92	0.091	0.063	29.10	*2011*	
6.5	51.22	41.25	46.70	160.91	0.118	0.065	33.41	*2009*	
7.5	48.41	39.94	43.55	154.21	0.073	0.069	31.29	*2008*	
8.5	47.04	37.91	43.17	148.18	0.137	0.064	30.70	**2007**	**0.29**
9.5	47.28	38.53	43.56	153.17	0.134	0.065	31.48	*2005*	
10.5	49.49	39.85	45.14	157.33	0.078	0.075	32.36	*2003*	
11.5	49.97	39.64	45.85	160.25	0.088	0.068	46.52	*2002*	
12.5	47.44	35.37	44.00	149.80	0.091	0.077	32.14	**2000**	**0.28**
13.5	52.18	39.25	47.22	162.17	0.126	0.090	35.50	*1998*	
14.5	53.00	39.69	50.28	168.52	0.115	0.089	36.86	*1996*	
15.5	51.58	38.04	47.72	158.31	0.116	0.099	35.37	*1994*	
16.5	52.04	38.69	50.45	163.93	0.142	0.095	36.63	**1992**	**0.26**
17.5	52.13	37.69	50.23	166.86	0.121	0.096	36.98	*1989*	
18.5	55.25	39.06	53.79	175.93	0.101	0.110	39.93	*1987*	
19.5	57.11	39.99	54.97	176.47	0.117	0.114	40.02	*1985*	
23	57.71	36.21	57.31	173.52	0.100	0.126	40.35	*1978*	
27	68.42	37.99	66.31	190.16	0.127	0.148	44.62	*1968*	
31	66.91	39.43	74.28	234.60	0.245	0.212	62.10	*1957*	
35	58.30	38.14	69.41	251.09	0.270	0.308	63.45	1947	**0.20**
39	52.74	39.99	61.89	224.54	0.230	0.292	60.05	1936	**0.20**
43	45.12	40.20	48.18	204.62	0.222	0.199	60.78	1924	**0.20**
49	42.36	39.38	45.17	177.63	0.107	0.107	55.92	*1904*	
53	43.08	40.03	39.59	157.80	0.110	0.060	47.48	**1891*	
59	40.45	37.99	34.52	129.09	0.098	0.041	37.71	**1871*	***0.20**
63	42.82	39.54	32.50	121.75	0.053	0.028	31.89	**1857*	***0.20**
53	45.74	43.80	40.01	155.38	0.084	0.048	46.54	**1891*	
59	42.87	40.92	37.68	142.92	0.081	0.042	42.13	**1871*	***0.20**
63	44.73	41.55	32.19	119.29	0.047	0.022	28.49	**1857*	***0.20**
67	43.49	40.14	28.51	100.75	0.098	0.016	21.79	**1841*	***0.20**
71	45.43	41.89	29.72	100.91	0.071	0.016	21.71	**1825*	***0.20**
75	44.35	41.21	27.55	94.26	0.042	0.013	19.77	~**1808*	
79	48.48	44.89	31.44	101.00	0.081	0.016	20.34		
84.5	39.45	36.09	24.27	92.28	0.063	0.015	20.40		
99.5	39.37	36.93	21.67	83.03	0.128	0.011	16.67	~early 18th century	
109.5	39.32	37.72	22.85	82.76	0.074	0.010	16.11		
119.5	40.94	37.95	22.80	83.77	0.081	0.009	16.53		
129.5	40.56	37.29	22.51	84.52	0.060	0.010	16.08	~early 17th century	

Radioactive Isotope Dating: Bold is directly dated, *italic* is interpolated, *asterik is extrapolated.

Red numbers are the highest peaks in the core

Appendix G: Trygve Braarud CTD graph of oxygen, temperature, chlorophyll fluorescence and salinity.

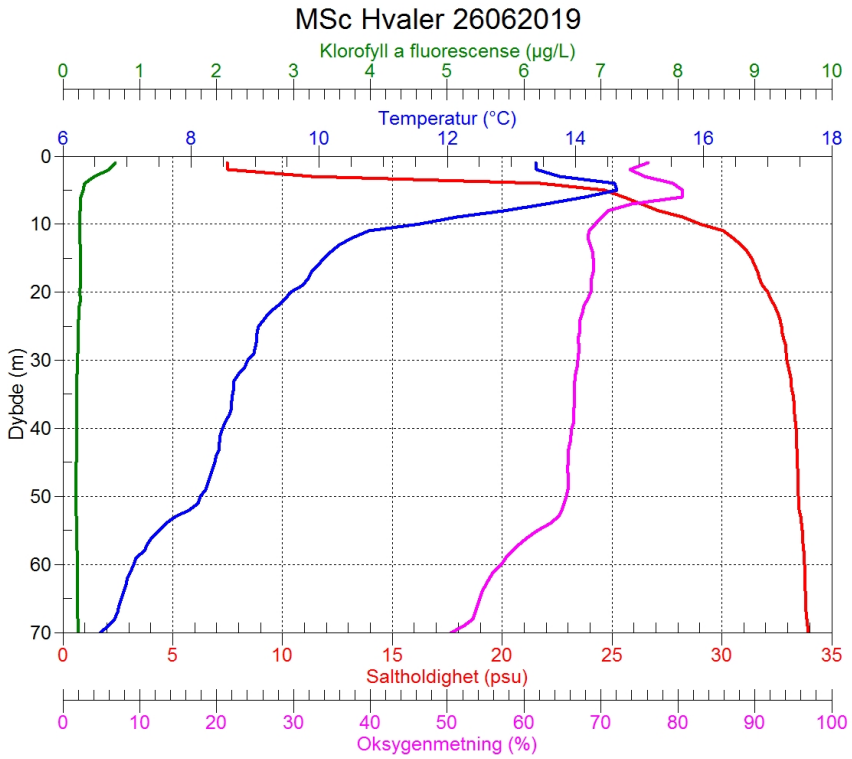

Appendix H: Raw data for TOC (%), TN (%) and C/N ratio

TOC Box # (JP-B#-M)	Interval	av.depth	W- empt. Tube [No lid] (g)	W- tube + sed (g)	W- sed only (g)	W- Sed + tube acid washed (g)	W-TOC smpl w/o TIC (g)	TOC Corr. Factor	TOC (%) measured	TIC (%) - (TC - TOC corr)	N (%)	TOC (%) corrected	Corrected C:N RATIO (TOC/TN)	TN (%)	TC (%)	Dates
1	0-1	0.5	11.516	12.537	1.021	12.254	0.738	0.977	2.86	-0.10	0.37	2.795	9.3	0.30	2.70	**2019**
2	1-2	1.5	11.518	12.528	1.010	12.280	0.762	0.980	2.89	-0.13	0.37	2.833	9.4	0.30	2.70	*2018*
3	2-3	2.5	11.517	12.493	0.976	12.250	0.733	0.981	2.73	0.02	0.35	2.677	8.9	0.30	2.70	**2016**
4	3-4	3.5	11.519	12.516	0.997	12.275	0.756	0.981	2.75	0.18	0.36	2.697	8.7	0.31	2.88	*2015*
5	4-5	4.5	11.519	12.555	1.036	12.314	0.795	0.981	2.94	-0.20	0.35	2.884	9.6	0.30	2.68	**2013**
6	5-6	5.5	11.501	12.486	0.985	12.268	0.767	0.983	2.68	0.01	0.34	2.633	8.8	0.30	2.64	*2011*
7	6-7	6.5	11.575	12.640	1.065	12.407	0.832	0.982	2.61	0.08	0.34	2.562	8.8	0.29	2.64	*2009*
8	7-8	7.5	11.517	12.491	0.974	12.273	0.756	0.983	2.55	0.10	0.33	2.505	8.6	0.29	2.61	*2008*
9	8-9	8.5	11.570	12.524	0.954	12.314	0.744	0.983	2.56	0.08	0.33	2.517	8.7	0.29	2.60	**2007**
10	9-10	9.5	11.495	12.524	1.029	12.298	0.803	0.982	2.61	0.04	0.34	2.563	8.8	0.29	2.60	*2005*
11	10-11	10.5	11.674	12.640	0.966	12.436	0.762	0.984	2.55	0.05	0.33	2.509	9.0	0.28	2.56	*2003*
12	11-12	11.5	11.487	12.482	0.995	12.267	0.780	0.983	2.54	0.07	0.33	2.496	8.9	0.28	2.57	*2002*
13	12-13	12.5	11.528	12.571	1.043	12.346	0.818	0.982	2.52	0.12	0.32	2.475	8.8	0.28	2.59	**2000**
14	13-14	13.5	11.482	12.528	1.046	12.302	0.820	0.982	2.52	0.12	0.32	2.475	8.8	0.28	2.59	*1998*
15	14-15	14.5	11.501	12.477	0.976	12.268	0.767	0.983	2.57	0.06	0.33	2.522	8.8	0.29	2.59	*1996*
16	15-16	15.5	11.552	12.543	0.991	12.328	0.776	0.983	2.56	0.06	0.32	2.516	9.0	0.28	2.58	*1994*
17	16-17	16.5	11.470	12.508	1.038	12.284	0.814	0.982	2.47	0.15	0.31	2.426	8.7	0.28	2.58	**1992**
18	17-18	17.5	11.553	12.551	0.998	12.338	0.785	0.983	2.46	0.14	0.31	2.418	9.0	0.27	2.56	*1989*
19	18-19	18.5	11.675	12.668	0.993	12.454	0.779	0.983	2.44	0.17	0.30	2.399	8.6	0.28	2.57	*1987*
20	19-20	19.5	11.517	12.526	1.009	12.311	0.794	0.983	2.41	0.15	0.30	2.369	8.8	0.27	2.52	*1985*
22	22-24	23	11.482	12.551	1.069	12.329	0.847	0.982	2.4	0.17	0.29	2.358	8.7	0.27	2.53	*1978*
24	26-28	27	11.521	12.601	1.080	12.374	0.853	0.982	2.52	0.09	0.30	2.475	9.2	0.27	2.56	*1968*
26	30-32	31	11.582	12.589	1.007	12.378	0.796	0.983	2.75	0.00	0.31	2.704	10.0	0.27	2.70	*1957*
28	34-36	35	11.484	12.478	0.994	12.278	0.794	0.984	2.72	0.03	0.30	2.676	9.9	0.27	2.71	1947
30	38-40	39	11.519	12.491	0.972	12.305	0.786	0.985	2.43	0.04	0.28	2.394	9.6	0.25	2.43	1936
32	42-44	43	11.532	12.534	1.002	12.359	0.827	0.986	2.26	0.05	0.26	2.228	9.3	0.24	2.28	1924
35	48-50	49	11.514	12.558	1.044	12.382	0.868	0.986	2.07	0.11	0.25	2.041	8.9	0.23	2.15	*1904*
37	52-54	53	11.618	12.679	1.061	12.506	0.888	0.986	1.98	0.11	0.23	1.953	8.9	0.22	2.06	**1891*
40	58-60	59	11.468	12.467	0.999	12.307	0.839	0.987	2.44	0.00	0.30	2.409	11.5	0.21	1.77	**1871*
42	62-64	63	11.532	12.509	0.977	12.353	0.821	0.988	2.52	0.00	0.31	2.489	12.4	0.20	1.65	**1857*
ABD 45	52-54	53	11.532	12.568	1.036	12.404	0.872	0.987	1.94	-0.08	0.20	1.915	9.6	0.20	1.83	**1891*
48	58-60	59	11.478	12.473	0.995	12.316	0.838	0.987	1.79	0.12	0.22	1.767	8.0	0.22	1.89	**1871*
50	62-64	63	11.520	12.497	0.977	12.342	0.822	0.988	1.84	-0.17	0.21	1.817	8.7	0.21	1.65	**1857*
52	66-68	67	11.457	12.436	0.979	12.281	0.824	0.988	1.54	0.00	0.20	1.521	7.6	0.20	1.52	**1841*
54	70-72	71	11.515	12.524	1.009	12.367	0.852	0.987	1.43	0.04	0.19	1.412	7.4	0.19	1.45	**1825*
56	74-76	75	11.571	12.593	1.022	12.434	0.863	0.987	1.39	0.12	0.20	1.372	6.9	0.20	1.49	*~*1808*
58	78-80	79	11.559	12.584	1.025	12.431	0.872	0.988	1.39	0.04	0.19	1.373	7.2	0.19	1.41	
60	82-87	84.5	11.495	12.490	0.995	12.332	0.837	0.987	1.36	0.24	0.19	1.343	7.1	0.19	1.58	
63	97-102	99.5	11.571	12.597	1.026	12.434	0.863	0.987	1.37	0.20	0.20	1.352	6.8	0.20	1.55	
65	107-112	109.5	11.456	12.526	1.070	12.366	0.910	0.987	1.34	0.18	0.19	1.323	7.0	0.19	1.50	
67	117-122	119.5	11.560	12.569	1.009	12.415	0.855	0.988	1.33	0.19	0.19	1.314	6.9	0.19	1.50	
69	127-132	129.5	11.530	12.580	1.050	12.415	0.885	0.987	1.61	-0.05	0.22	1.586	8.3	0.19	1.54	

Grey color means overlap between JP-19P and JP-19Abd